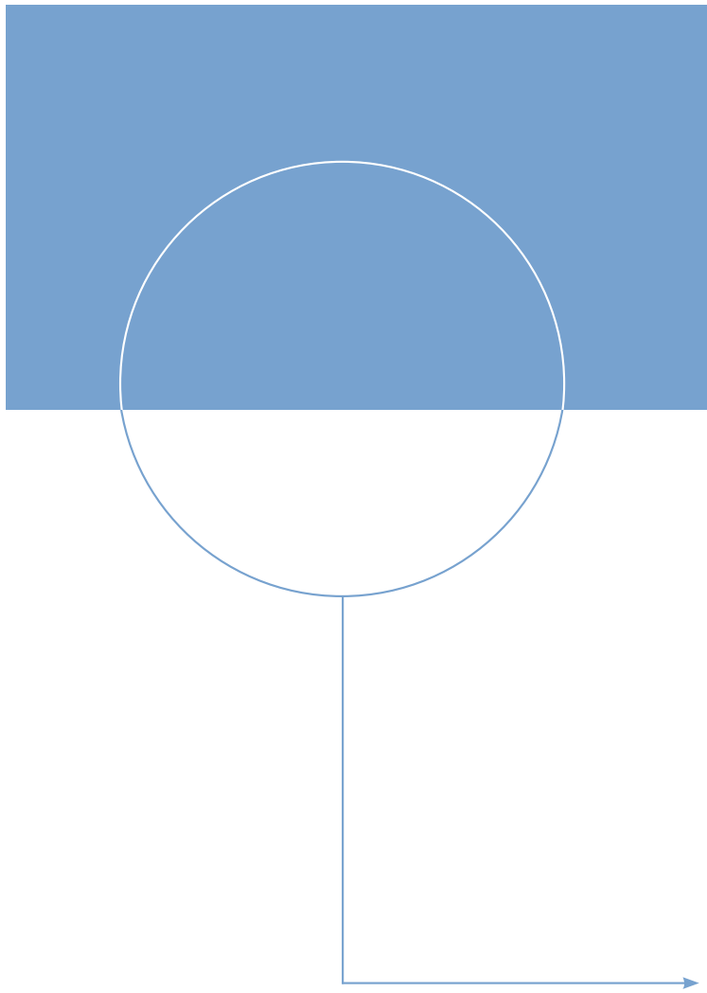

Master's thesis

2022

Bjorn Haver

NTNU
Norwegian University of
Science and Technology
Faculty of Engineering
Department of Manufacturing and Civil Engineering

Bjorn Haver

Investigation of manufacturability of grid structures of the structural part of Flying V using additive manufacturing

September 2022

NTNU
Norwegian University of
Science and Technology

NTNU
Norwegian University of
Science and Technology

NTNU

Norwegian University of
Science and Technology

Investigation of manufacturability of grid structures of the structural part of Flying V using additive manufacturing

Bjorn Haver

Master in Sustainable Manufacturing
Submission date: September 2022
Supervisor: Sotirios Grammatikos

Norwegian University of Science and Technology
Department of Manufacturing and Civil Engineering

Acknowledgements

I would like to thank my supervisor Prof. Sotirios Grammatikos for all the help and insight during the period of this master thesis work, and for introducing me to the people of TU Delft. Thank you for motivating me and giving me the chance to work on this project.

Big thanks to Asst. Prof. Jos Sinke for his professional guidance, recommendations and allowing me to work on the Flying V project from Norway.

Special thanks to Chaman Srivastava for helping me to gain a better understanding of the testing equipment and results of the CT Scan and motivating me every day by providing helpful new insights when required. I appreciate all the conversations we had and the late afternoon coffees at 5 PM.

Thanks to all my teachers at NTNU Gjøvik for motivating me and acquiring me with a lot of new knowledge.

The biggest thanks to my family and girlfriend for their support and strong belief in me.

Abstract

The awareness of climate change is raising among all sectors - including aviation. In order to reduce the global impact of aviation, fuel usage should be reduced drastically. TU Delft designed a new configuration for an aircraft where the fuselage and the wing consists of one part. This new design is estimated to decrease fuel usage by 20%. The engineers plan to use composite material for the manufacturing due to their excellent specific properties. Currently, grid or lattice structures are used to give strength to a part made of composites. Grid structures consist of a rib and skin and are used to increase mechanical performance of aircraft structures while keeping the weight low. However, traditional manufacturing methods of grid structures have one disadvantage in common - the excessive fiber build up at the node where the ribs meet.

This master thesis took place at the premises of ASEMLab - Laboratory for Advanced and Sustainable Engineering Materials Research - and employs a new technology for additive manufacturing of composites. It tried to study the feasibility of this method for the production of grid structures. This manufacturing technique is focused on a dual-nozzle system where the fiber and thermoplastic are extruded from two different nozzles. Furthermore, the nozzle can alter pressure on the fiber during printing making it possible to have grid structures with continuous fibers through all nodes.

In this project different specimens were manufactured representing a grid structure - both with carbon fibre reinforcement and without (pure plastic). These samples were exposed to testing and different analyses to evaluate the printing and structural quality. Results of the tests were used to discuss if the reinforcement offered a significant advantage. Limitations and challenges were discussed as well as the advantages over traditional methods for composites and alternative additive manufacturing methods for composites. To conclude, the proposed method offers great potential over conventional methods and if developed well it can be used for the manufacturing of grid structures.

Keywords: additive manufacturing, composites, grid structures, continuous fibers.

Contents

Figures

Tables

Acronyms

AFP automated fiber placement.

AM additive manufacturing.

ATL automated tape layup.

CFC continuous fiber coextrusion.

CFF continuous fiber fabrication.

CFRP carbon fiber reinforced plastic.

CT x-ray computed micro-tomography.

CTE coefficient of thermal expansion.

FDM fused deposition modeling.

FW flying wing.

L/D lift-to-drag.

PAN polyacrylonitrile.

PETG polyethylene terephthalate glycol.

1 Introduction

The importance of sustainability is growing in all industries, including aviation. The aviation industry is one of the few sectors where energy consumption increased, while the production decreased [1]. Air traffic affects the environment and humans on all scales [2], at a local level near airports through noise and air pollution, at a regional level, and at a global scale through climate change. It is estimated that aviation contributes around 5% to climate change [3] and without radical action this number is expected to increase.

One method to reduce the climate change impact of aviation is to create a more efficient design of an airplane that requires significantly less fuel. A flying wing (FW) is an airplane configuration where the fuselage and wing are integrated and combined into one component [4]. According to Bolsunovsky *et al.* [4] this design provides an increased L/D ratio of approximately 20% compared to conventional aircraft designs. The original Flying V designed by Benad [5] is shown in fig. 1.1a[1] and has the same size and passenger capacity as an Airbus A350. This design is further developed at TU Delft in the Netherlands through different projects, including engine location [6], cockpit design [7], and design optimization [8].

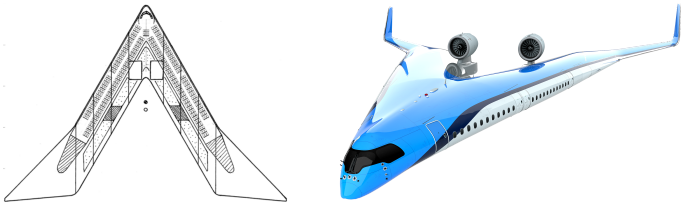

(a) **(b)**

Figure 1.1: (a) First sketch of the configuration and (b) Flying V design TU Delft

Fig. 1.1b[2] shows a visualization of the current design. As the fuselage and the wing of the aircraft consists of one part, the whole structural design is based of ribs and spars as shown in fig. 1.2. This is considered a typical grid and applied in different structures for added strength and stiffnesss. Currently, one method to manufacture grid structures is by using composites. However, according to Wu *et al.* [9] excessive fibers build up at the nodes of these grids which causes imperfections and local thickening. A method to overcome this is through AM as suggested by Forcellese *et al.* [10]. In their study short fibers were chosen as material, as opposed to continuous fibers. New technologies enable to manufacture continuous fiber carbon fiber reinforced with thermoplastic layer-by-layer. One of the methods to achieve this is by using two extruders, also referred to as continuous fiber coextrusion. This project aims to proof the concept of CFC for manufacturing of grid structures.

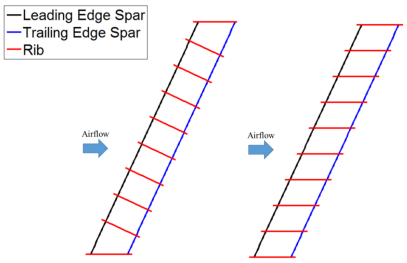

Figure 1.2: Design textbook rib orientation for a swept back wing [11]

[1] J. Benad, 'The flying v-a new aircraft configuration for commercial passenger transport,' 2015
[2] `https://www.tudelft.nl/en/ae/flying-v`

1.1 Problem Domain and Boundaries

It is important to understand the areas of investigation of the thesis. Considering the description above, the project focuses on the following areas:

- The advantages and challenges of lattice structures manufactured with composites;
- The advantages and challenges of using additive manufacturing for the fabrication of composite grid structures.

Through this master thesis more knowledge is gained on the areas of additive manufacturing and grid structures. This supports the recommendation of the discussed technology for structural components and helps to prove the concept. The project focuses on the following subjects:

- The role of composites on the development of structural components for aircraft;
- The development of additive manufacturing technologies for composite materials.

In order to distribute time efficiently certain boundaries are set related to the subjects. The project is focused on one set of parameters for the manufacturing of the components. There is no large improvement of the parameters involved in the experiments and only one type of thermoplastic is used (PETG). Furthermore, due to the complex nature of continuous fibers, the simulation is solely focused on structural behavior. The testing is done by quasi-static tests and measures tensile strength.

1.2 Research Questions

This project aims to proof the concept of continuous fiber coextrusion (CFC) for the manufacturing of grid panels as used in aircraft wings. A common problem in the manufacturing of grid structures with carbon fiber reinforced plastic is excessive fiber build-up at nodal points which has a negative impact on the mechanical performance. The following questions are answered through the execution of this study:

1. What are the conventional manufacturing methods for lattice structures and what are the problems?
2. How is the continuous fiber fabrication different from other (additive) manufacturing methods and how can it solve the current challenges?
3. What is the influence of PETG impregnated with continuous carbon fibre on the tensile strength of node points?
4. What are the limitations of CFC?
5. How can this technique be applied on a large (industrial) scale?

1.3 Thesis Outline

This thesis describes the investigation of possibilities of producing a grid structure through additive manufacturing. In chapter 2 the theoretical background of the different topics are covered to assist with answering the research questions as described in section 1.2. Chapter 3 covers the scientific methodologies used for this project and demonstrates the creation of the design, simulation, and different experimental tests. In chapter 4 the results and discussion are written, where the outcome of the tensile tests and CT scan are accurately analyzed. Lastly, the conclusion is drawn in chapter 5 accompanied with a suggestion for future work.

2 | Theory

2.1 Flying V

The idea of a flying wing is not something new of the last years. During the Second World War researchers already expected that an aircraft without fuselage and tail results in a low drag coefficient [6]. It was discovered this is caused by higher Reynold number on the wing, induced drag due to absence of a horizontal tail, and a reduced static margin [4]. As the classical aircraft design of separate wing and fuselage is already optimized, flying wings are the new invention towards the impact of aviation on climate change [6, 8].

The most important reason advocates of the flying wing bring up is the gain of around 20% in aerodynamics, reducing the climate impact [12]. However, van Empelen & Vos also write that certain problems have to be solved before the flying V is departing. First of all, there is stress issues present in the nose region where the two wings meet [13]. Dotman [13] discovered that this is due to increase of thickness which generates high local stresses caused by the changing angles and cross-section of the aircraft. One option to reduce the stresses is through introduction of lattice or grid structures. Typically, isogrids are used in aircraft configurations since it is highly efficient in distributing loads within a structure [14]. The next section elaborates on grid structures and their mechanical behavior.

2.2 Grid Structures

In the manufacturing of aircraft configurations it is essential to minimize the weight of the structure while maintaining sufficient mechanical performance. Therefore, isogrid structures are typical for aircraft configurations as it provides high efficiency in the distribution of loads, offers great buckling resistance and is less affected by impact damage, crack propagation, and delamination [14] as discussed in the last section.

The precursor of the Boeing company holds the patent for the first isogrid structure [15]. The grid shows isotropic behaviour in the plane of the structure [16]. This first structure was manufactured using a single piece of aluminum and consists of a skin with stiffeners as displayed in fig. 2.1. Typically, these stiffeners run in 2 to 4 directions and form a repeating pattern [15]. However, the isogrid structures manufactured with aluminum alloys requires expensive processes with long manufacturing times and a large amount of material waste [10]. The introduction of carbon fiber reinforced polymers allows to manufacture isogrid structures with improved performance and efficiency compared to aluminium structures. These grids are manufactured with continuous unidirectional fibers [17] that create a stiff and strong structure.

The manufacturing of isogrid structures is complex due to material build-up at the intersecting nodes where the ribs meet. In order to achieve the best mechanical performance it is necessary to have continuous fibers along all ribs. However, at each intersection, three times the amount of fiber builds up leading to higher load concentrations at those locations and premature failure [14]. Furthermore, according to Kim it contributes to warping of the plates during manufacturing due to the coefficient of thermal expansion (CTE) between the fiber and the resin. Therefore, it is required to design a special strategy specifically for the nodal points in isogrid structures. In the study of Güemes *et al.* [18] three different methods are designed as visualized in fig. 2.2. The first design has an offset to avoid having excess fiber build-up. The triangular void is often filled up with resin [14]. The last design has two fibers that are discontinued in order to limit the build-up of fiber. It is expected that through CFC it is possible to achieve a stiffener node with continuous fibers running

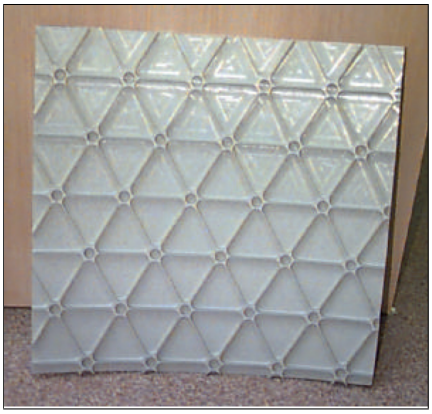

Figure 2.1: Aluminum isogrid panel [15]

through all ribs.

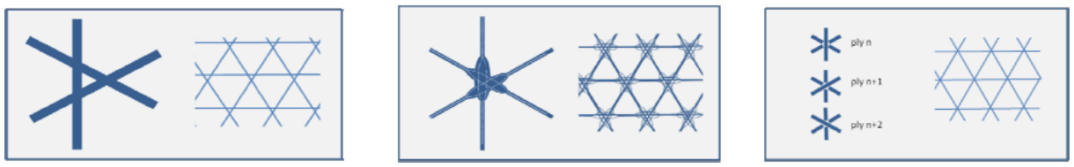

Figure 2.2: Three different solutions for the nodal point of composite isogrid structures [18]

2.2.1 Behavior of Grid Structures

Huybrechts and Tsai [19] investigated the behavior of grid structures to identify critical points. Their findings are discussed in this section.

The first parameters of major influence is the thickness of the ribs. Rib buckling is an issue often occurring with thin ribs - a phenomena where the ribs bend perpendicular to the direction of the force. Usually there is a large decrease in compressive strength for thin ribs, but when exposed to tensile load buckling of transverse ribs takes place. The advantage of decreasing the width of the ribs is the decrease in material failure. Adding an extra rib may increase the failure strength, but makes nodal points more complex. The angle of the ribs influences the shear strength of a lattice structure. The steeper the angle, the higher the shear strength.

Despite the name suggests it, isogrid structures are not isotropic. With decreasing thickness of ribs comes an increase in rib buckling as aforementioned. Furthermore, isogrids show more resistance to tensile loads than to compressive loads. A combination of compressive loads along the axial ribs and transverse tensile loads often cause the most buckling problems.

As mentioned before, one nodal point strategy is to create an offset. However, this offset has a noticeable effect on the grid's strength. The issue becomes more present with thinning of the ribs. Especially for cylindrical lattice structures the effect of the offset becomes more complex. Despite the offset reducing material failure, it increases buckling failure loads. It is expected that through producing nodal points without offset and continuous fibers in all ribs both material strength and structural strength are achieved.

2.2.2 Manufacturing Technologies for Isogrid Structures

Isogrid structures are often used in aircraft configurations that feature a cylindrical or conical shape. In order to manufacture those structures with composites the correct manufacturing method is required. Manual layup is an accurate method to manufacture complex parts because humans are able to sense and see the part as opposed to robots. However, for large aerospace structures manual layup is not efficient which introduces different manufacturing technologies. Four methods are discussed now which are automated fiber placement (AFP), automated tape layup (ATL), autoclave and filament winding.

Automated Fiber Placement

Fig. 2.3 shows a schematic demonstration of the filament head in the AFP process. The manufacturing systems consists of a multi-axis robotic arm or gantry with a fiber placement head attached to it. The required shape of the part that is to be manufactured defines the tool that is most suitable. For large plates a gantry machine is desired, while complex shapes usually require the use of a robotic arm [20].

In the process, prepeg tows are fed to the fiber placement head that lay down the tows in a mould to form a continuous prepreg layer [21, 22]. The AFP tool features different components as visualized in the image. The compaction roller ensures placement of the tows and reduces voids, which is often a defect in composite structures [23]. It is possible to clamp, cut, and restart an individual tow in the process with the cutter tool which makes it suitable for the manufacturing of complex geometries [24]. Both thermoset and thermoplastic are suitable as material for the AFP process being impregnated tows or slit prepreg tape [24, 25]. Especially for thermoplastic material extreme heat is required for proper adhesion [20] which is produced by the infrared lamp. Other options for heat production are laser heaters [26], or gas torches [27]. Often there is a system present for cooling of the material as well. Not only temperature ensures adhesion, but the compaction and tension caused by force of the roller establishes a strong connection between the layers of tape. [20, 24].

The process allows tows to be laid in programmed positions and orientations to manufacture a laminate with the required strength and stiffness [21]. According to Dirk *et al.* [24] the process is limited by the steering radius which causes imperfections such as ply wrinkling and tool detachment. Therefore, it is necessary to cut the tow when the steering radius is too small leading to discontinuous fibers. When AFP is used for the manufacturing of lattice structures a strategy for the nodes is chosen as visualized in fig. 2.2.

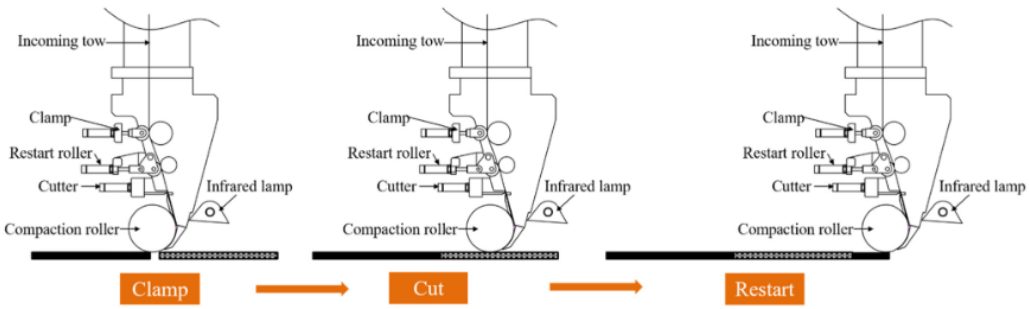

Figure 2.3: "Clamp-Cut-Restart" operation of AFP [22]

Automated Tape Layup

Automated tape layup is similar to automated fiber placement. However, ATL is more suitable for flat plain surfaces while AFP is applied with more complex geometries [21]. Fig. 2.4 shows an illustration of the ATL layup head. Dirk *et al.* [24] describe the process: a piece of tape is attached on the tool. Thereafter, the system accelerates to start the layup process. During the process, material is attached to the tool using force that is transferred again to the roller. The ATL head controls the correct pressure distribution is applied during layup. This ensures tension in order to avoid tearing, enables layup in slightly curved geometries and improve alignment of the plies. Temperature is controlled by the heating zone.

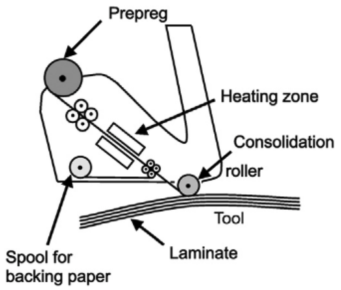

Figure 2.4: Schematic of an ATL layup head [24]

Robotic Filament Winding

Fig. 2.5 shows a schematic representation of the traditional filament wending technique. Advanced composites are produced using fibres that pass through a resin bath before being winded on the mandrel. This mandrel rotates to ensure the impregnated fiber is draped on the whole part. Different production parameters are the angle of the mandrel and the rotational speed [28]. After curing of the material the mandrel is typically removed. Complex shapes are achieved through this process as the geometry of the mandrel is configurable. Examples of products that are manufactured through filament winding are turbines or aircraft fuselages. Robotic filament winding consists of the same technique but involves a robotic arm to execute the winding and influence the rotation [28]. This introduces advanced winding patterns and more flexible manufacturing processes. Currently, filament winding is the most used technology for the manufacturing of lattice structures [29]. The introduction of additive manufacturing for composite materials enables the production of lattice structures with complex and irregular shapes as suggested by Azarov *et al.* [29].

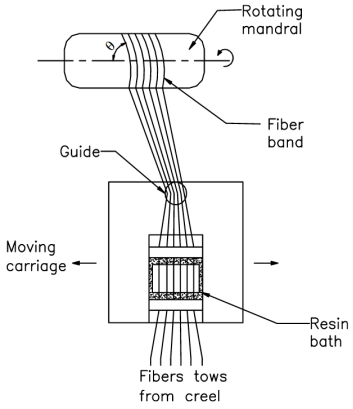

Figure 2.5: Schematic of the wet filament winding process [30]

Autoclave

The fourth and last method for the manufacturing of composite aircraft structures is called autoclaving [31]. Fig. 2.6 shows an example of an industrial autoclave [1]. Traditionally, it start with layers of carbon fiber impregnated with an uncured resin. These layers are laid upon a tool which form a laminate together. This laminate is placed in an autoclave often enclosed in a vacuum bag. In the oven, the temperature is increased while a vacuum is drawn in the bag. The pressure that is caused by this technique forms the laminate around the shape of the tool and presses out excess resin. Furthermore, this pressure reduces porosity, which is often a defect in parts manufactured with prepreg material [31]. The temperature ensures a reduction of the viscosity of the resin which makes it easier to flow and wet the reinforcement. After curing in the autoclave a solid and stiff part is produced.

Figure 2.6: Typical industrial autoclave

2.3 Continuous Fiber Fabrication Technologies

The equipment used in this study introduces new advanced technologies that are discussed in section 2.4. In this section the alternatives are described to see how they relate to eachother.

CFC is a technique of additive manufacturing - often referred to as 3D printing - where a part is produced through layer-by-layer deposition. The most common technique is fused deposition modeling where the material used is thermoplastic resin [32]. However, this resin shows poor performance and this was initially solved by reinforcing the material with e.g. chopped fibers [33]. The mixture of thermoplastic resin and the reinforcement that came out of the extruder showed an increase in mechanical properties, but was highly dependent on the volume fraction and orientation of the fibers [34]. Therefore, the CFF technique was introduced, where the reinforcement and matrix are separately fed into the extruder and the fibers are aligned. The process of additive manufacturing consists of steps conforming:

- Design of the component in CAD software;
- Converting the design to a .stl file that can be read by the slicer software;
- Slicing the component with the desired parameters to create the model that is split up by different layers;

[1] https://www.aac-autoclave.com/sale-2363594-temperature-laminated-chemical-industrial-autoclave-auto-clave-machine-html

- Exporting the sliced model as a G-code. G-code is a language that is read by 3D printers involving all the information necessary to print the model. E.g. printing directions and printing speed;
- Uploading the G-code to the printer and starting the print with the desired filament;
- Removing the part from the printing bed with the help of a scraper;
- Removing excess material from the part e.g. strings, brim or supports.

2.3.1 The Mechanisms

Fig. 2.7 shows two methods of the printing process, with a single nozzle and dual nozzles. The first method (fig. 2.7a) is commonly used on modified FDM printers since they only have one extruder. The thermoplastic and fiber are both fed into the same nozzle. Due to the heated nozzle, the polymer melts and forms the matrix. When the material touches the printing bed it solidifies and that is how objects are created [34]. However, the downside of this method is the short impregnation time which leads to uneven fiber/polymer distribution and voids in the fiber filaments [32]. The advantage is that only one piece of equipment is required which improves the mechanical performance significantly when compared to an object created of chopped fibers reinforced with thermoplastic [34].

The second method (fig. 2.7b) offers more flexibility and customization for the printing process. Contradictory to the single nozzle method, these printers makes it possible to choose layers or positions to reinforce while leaving other layers without reinforcement [35]. In this technique the continuous fiber is integrated with plastic while the thermoplastic filament is coming through the other extruder to promote the bonds. Usually this process has a cutter in the fiber nozzle to cut between layers, between paths within a layer and at some special locations to increase surface quality [35]. According to Chen *et al.* this method eliminates the problems the single nozzle has with uneven distribution of fibers and polymers and the creation of voids. Furthermore, it reduces material cost as it can be decided when to turn a nozzle on or off in case of required reinforcement [34]. This technique is used by the printer which is discussed later.

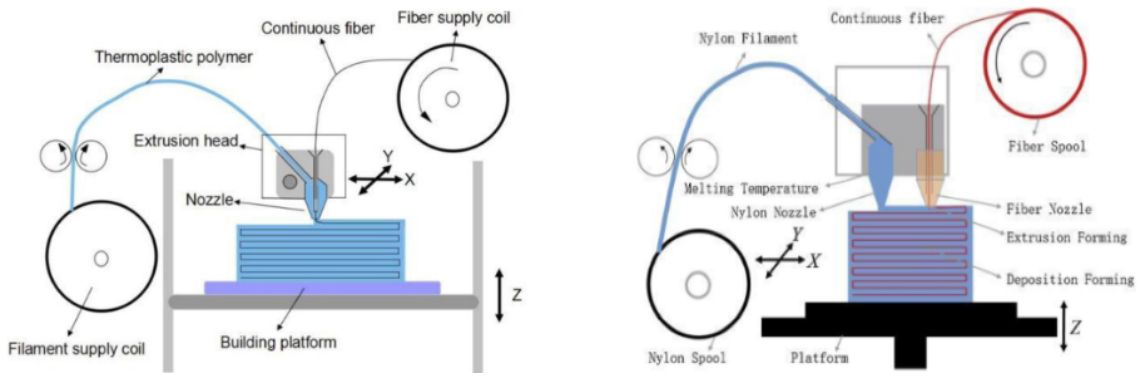

(a) **(b)**

Figure 2.7: Schematic Representation of the CFF Process With Single Nozzle (a) and Dual Nozzles (b) [34]

Besides the two methods described above, other techniques and printers to produce CFF objects exist as well. According to Zhang *et al.* [32], one method is based on the single nozzle principle with an in-situ laser to remove the voids discussed earlier. Fig. 2.8 shows a schematic representation of this technique. Due to the heat created by the laser close to the nozzle, the amount of voids are reduced and stronger bonds are created between layers [36].

Another method tried to solve the problems a single nozzle printer causes by adding a pressure roller close to the extruder [37]. The squeezing of the printed layer increased the bonding between the layers significantly according to the researchers. However, when the pressure got too high the

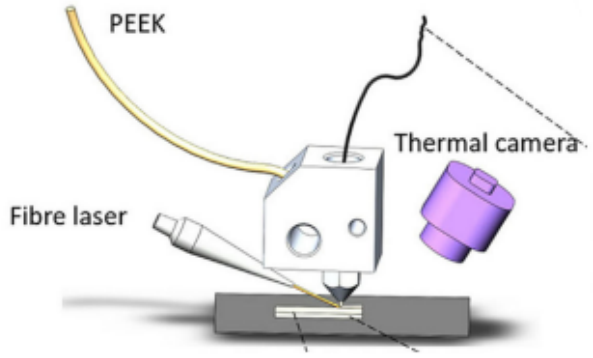

Figure 2.8: Schematic of the Printing Process Combined With Laser In-situ and Local Preheating [32]

printing accuracy decreased and could even cause printing failure [32].

Polymer filament has high manufacturing costs and is therefore not preferred [32]. Fig. 2.9 shows a printer principle which is based on polymer pellets with screw extrusion. The extrusion force from the screw allows melting of the polymer due to the high pressure and temperature [38]. Furthermore, for filament printing the fiber content is limited due to the reliance on the drag effect of the fiber and thus limits the performance of the produced composite [32]. Liu *et al.* [38] created a printer with in-situ microscrews and rollers to print composites. With high fiber content (> 50 wt%) the authors managed to extrude the polymer smoothly with the extrusion force. However, due to the material being pellets or powder, air can come into the printer which can cause defects in the objects to be printed [32].

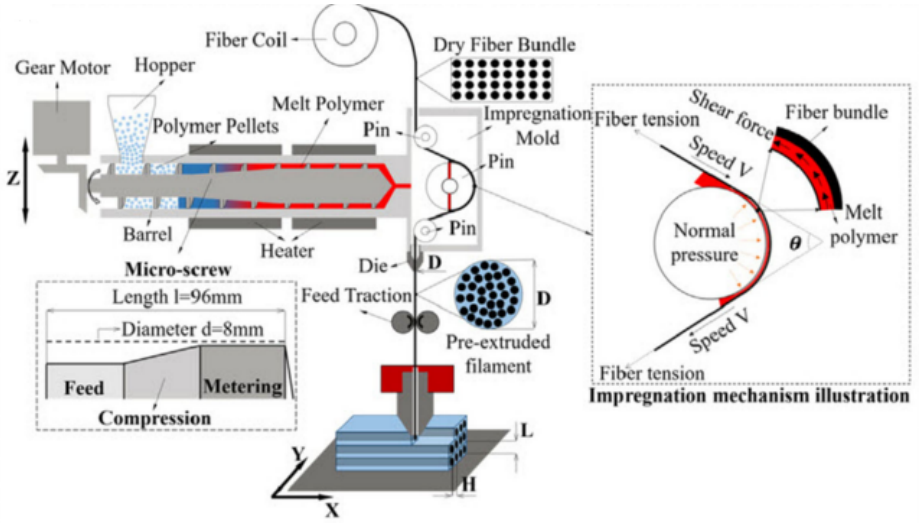

Figure 2.9: Schematic of Printing CFRPCs Based on Micro Screw [32]

2.3.2 The Materials

In principle, two materials are chosen during the production process of the composite through printing. On one side it is the reinforcement material and on the other side the matrix [34]. This can be both fed in the same extruder where the materials are combined through heat and impregnation or separately through two extruders. In order to select the right material for the product different perspectives should be considered.

In literature, mainly six materials are considered for the reinforcement. Carbon fibre, Kevlar, and glass fibre are the materials used the most. For the selection of the matrix material, it is important to consider three factors; physical factors (good bonding), chemical factors (no chemical reaction between fiber and matrix) and thermal factors (consider coefficient of thermal expansion and similar behaviour) [34]. Besides these factors the processing and preparation of the filament is of importance. For processing, melting temperature, viscosity, and solidification are essential factors. For filament preparation, polymer morphology, softness, filament stiffness, dimensional consistency, brittleness, and winding on spool are considered important according to the authors. Furthermore, polyamides are preferred due to their fast cooling characteristics. The filament that will be used for printing should have even diameter throughout and be parallel wound on spool to minimize the strain.

It can be concluded that a large amount of factors are important to consider when selecting a material. Carbon fibre is the widely used choice for the reinforcement according to the literature. When choosing the matrix it is essential to consider the physical, chemical, and thermal factors. Besides that proper processing and preparation of the filament is essential. The four perspectives in terms of economics, environment, social, and physical can assist in choosing the correct material for the task by assigning scores to different material. In the end, it is important to consider what materials the printer can print, as not every 3D printer can process all materials.

2.3.3 The Printing Directions and Mechanical Performance

The advantage of 3D printing is that a predesignated path can be designed which will be followed by the nozzle. It is well-known that the fiber direction determines the physical properties of the produced composites. Therefore, it is concluded that the printing direction will influence the mechanical properties to a large extent [39]. Furthermore, the advantage of 3D printing is that the fiber orientation can be changed for each individual layer. In this section different printing directions will be discussed including their influence on the mechanical properties.

Araya-Calvo *et al.* [33] provides an example of two different printing directions called concentric (fig. 2.10a) and isotropic (fig. 2.10b). Kabir *et al.* [34] defines different orientations mentioned in literature for the isotropic orientation: 0°, 30°, 45°, 60°, 75°, and 90°.

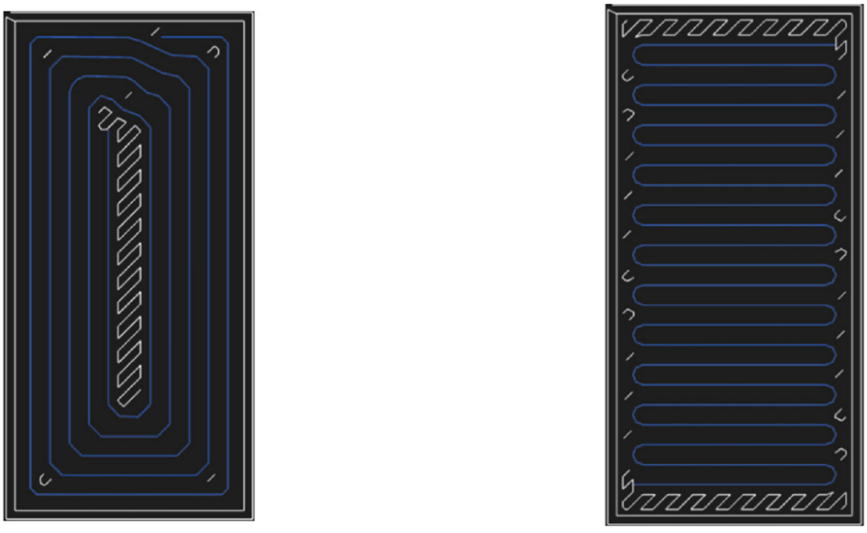

(a) **(b)**

Figure 2.10: Fiber Reinforcement Types, Concentric (a) and Isotropic -0° Layer (b) [33]

The authors investigated the influence of the orientations on the tensile strength of the composites with different fiber volume fractions produced with a Markforged printer. The composite with a V_f of 27% and orientation 0/0 achieved the highest tensile strength of 719 MPa. The composite with a FVF of 10.92% and orientation 15°/45°/75° had the lowest tensile strength of 64 MPa. Kabir *et al.* [34] conclude that the isotropic orientation with zero degrees, has the highest tensile properties which gradually decreases by increasing the angle. However, the fiber volume fraction has a large influence on the mechanical properties of a composite and this influences the tensile strength according to the rule of mixture [40]. Furthermore, Kabir *et al.* [34] claim that isotropic orientation is more stable against tensile and flexural loads than concentric orientation.

2.4 Continuous Fiber Coextrusion

In this project the Anisoprint Composer A4 is used to manufacture the parts. This printer is based on an open system - which means that one is not bound to one specific selection of materials. Furthermore, it allows for flexible fibre volume ratio and determination of fibre path trajectories. The printing bed is as large as an A4 paper sheet. With the CFC printer, it is possible to produce parts that are 30 times stronger than plastic while remaining two times lighter than aluminum [2]. In this section the printer and its features are discussed.

2.4.1 The Mechanism

The machine in this project features two extruders as shown in fig. 2.11[3]. The left part uses thermoplastic material as filament. The right part uses both fiber and thermoplastic filament. In this extruder a cutter is present to cut the fibers between layers and to ensure surface quality at specific locations in the print. The thermoplastic is melted and covers the fiber to create CFRP. This method reduces material cost as material usage is accurately controlled by the two extruders [34].

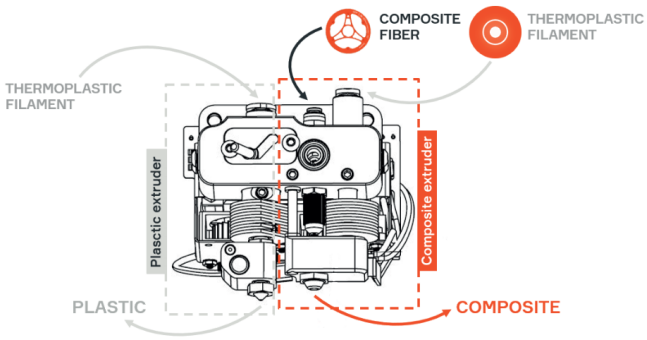

Figure 2.11: Schematic representation of CFC process

It is possible to use any thermoplastic material, even though it is recommended to use the same filament in both extruders. The carbon fiber filament used in this project is cured, impregnated and dried by the supplier which creates stiffness sufficient to be grabbed by the feeder. The pre-impregnation also increases the adhesion performance. The fiber filament is round which reduces the chance of folding and curling issues during change of nozzle direction. This means that CFC allows free fiber paths in all directions in contrast to e.g. AFP. The fiber used in the printing process has a thickness of 0.35 mm. A part printed with a layer thickness of 0.35 mm features bad surface quality and low amount of details. Therefore, the supplier of the printer invented a technique described

[2] https://anisoprint.com/solutions/desktop/
[3] https://support.anisoprint.com/composer/manual/

as marcolayer technology. Fig. 2.12[4] provides a visualization. The external shell which is visible to the eye consists of a small layer thickness to provide good surface quality. The inside featuring the reinforced perimeters is build of layers with a thickness of 0.36 mm. This enables manufacturing of a part with smooth outer layers and strong reinforcement.

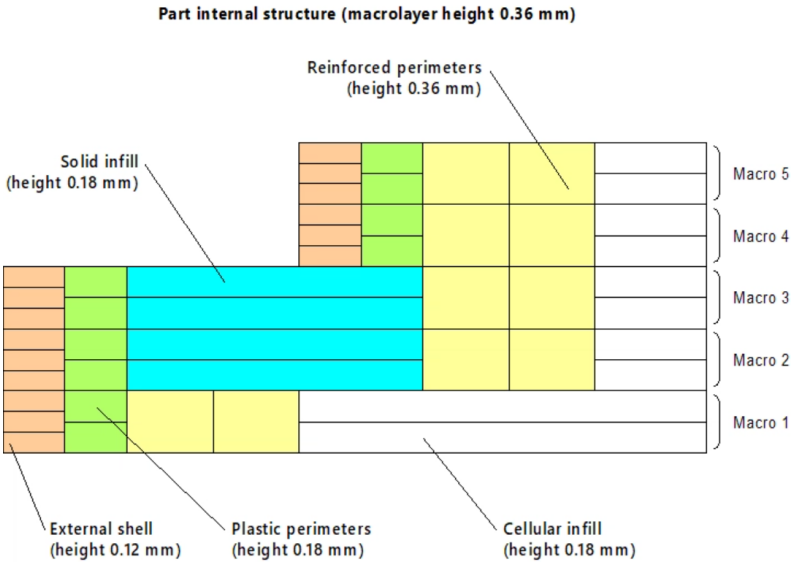

Figure 2.12: Marcolayer technology

As discussed before, the largest challenge of the manufacturing of lattice structures lies in the nodal points. Most 3D printers use pre-impregnated carbon fibre as filament such as the Markforged [41]. This creates severe fiber build up at the meeting points of the ribs (nodes) eventually leading to failure of the print since the printer head moves into the bump. The CFC method introduced a technology best described as fiber reshaping as visualized in fig. 2.13. In this process, the extruder applies pressure during extrusion, causing consolidation of the last deposited filament on top of the material. This creates an elliptical shape for the fiber and allows for a low layer thickness [42]. By changing the amount of thermoplastic added per piece of fiber the shape is altered and the fiber volume fraction is influenced. Not only does the consolidation allow for a lower layer thickness, but it also enables good layer adhesion. This technique is what makes the printer innovative [5].

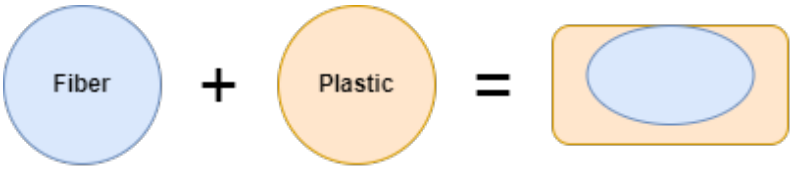

Figure 2.13: Fiber reshaping

[4] https://www.aniwaa.com/review/3d-printers/review-anisoprint-composer-a4-continuous-fiber-3d-printing/
[5] https://anisoprint.com/trainings/what-is-anisoprinting/

2.4.2 The Parameters

The most important parameters in the printing process are listed below as described by Chen *et al.* [35]:

- Layer height: defines the height of each printed layer, also influences the amount of layers. A larger layer thickness will provide a faster printing time but less details in the end product. For the CFC printer there is a special layer height pattern as displayed in fig. 2.12;
- Infill pattern: different infill patterns and density exist. The current method features five infill patterns as shown in fig. 2.14[6]. The patterns are called: solid, rhombic, isogrid, anisogrid, and reinforcement around the perimeters. The density influences printing time and mechanical performance. E.g. a solid part is significantly heavier than a hollow print, but has higher mechanical strength;
- Infill orientation: the orientation of the fibers is determined in terms of the angle which influences fatigue performance [43];

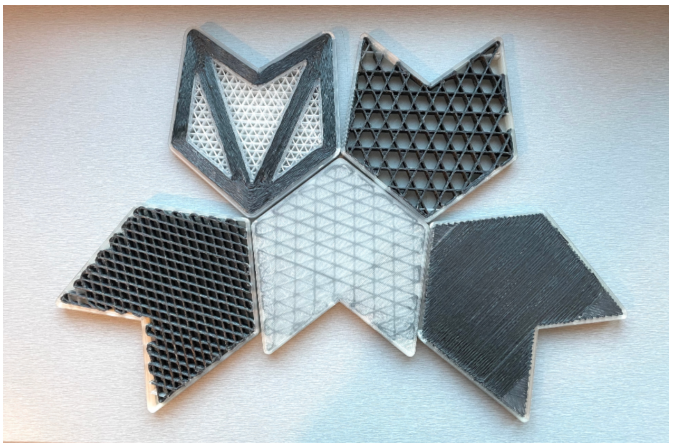

Figure 2.14: Five infill patterns offered by the supplier

Additionally, parameters are defined by Parmiggiani *et al.* [44] and Quan *et al.* [45]:

- Temperature of printing head: the correct temperature is important to ensure a strong bonding and to acquire the correct material properties. The optimal temperature differs per material and is provided by the supplier of the filament;
- Temperature of printing bed: the temperature of the printing bed affects the adhesion of the part to the bed.
- Fiber type: the type of fiber/material that will be used during the printing process. Dependent on the requirements of the product;
- Printing speed: the speed of the motors in the nozzle. When the speed is too high it can cause overheating due to limited cooling of the material. Too low speed can cause overheating because the nozzle is sitting on the same position too long [34]. Both cases cause print deformations. More on typical printing defects later.

The Aura slicer software features more advanced parameters. E.g. it enables the possibility to mask a certain area of the part to ensure fiber placement in a certain area as shown in the top left part in fig. 2.14. However, in this study these parameters are not used due to the complexity.

2.4.3 Materials

The prototype in this study is manufactured using the carbon fiber in combination with polyethylene terephthalate glycol (PETG). The carbon fiber spool is produced through a couple of steps described

[6] https://www.aniwaa.com/review/3d-printers/review-anisoprint-composer-a4-continuous-fiber-3d-printing/

below:

1. The carbon fiber filament consists of multiple monofilaments made of polyacrylonitrile (PAN). Together, these are heated three times. The first heating takes place at 400 °C and is called stabilization to stretch the PAN.
2. Next, the material is heated at 900 °C and is called carbonization as it removes the non-important elements in the filament.
3. After carbonization, graphitization takes place at a temperature of around 2800 °C and re-arranges the crystalline structure. After this step a carbon fiber tow is created.
4. This dry fiber tow is pre-impregnated with a special thermoplastic binder described as $[[C_{15}H_{16}O_2]_m[C_3H_5CIO]$ [46]. This composite is then cured which results in a stiff fiber and is rolled on a spool to be used for printing. In the end the filament has a fiber volume fraction of around 60%.

The produced filament is 30 times stronger and stiffer than normal plastic while being 7 times lighter than steel [7]. The carbon fiber is impregnated with the PETG during the printing process. Another possibility that is used by other printers is to use pre-impregnated carbon fiber without the addition of an extra thermoplastic that impregnates during printing. This process melts the thermoplastic surrounding the fiber in order to deposit it on the printing bed. This improves the adhesion and enables good impregnation, but the fiber volume ratio remains constant and shapes are limited (lattice structures become an issue). Impregnating the fiber during printing causes adhesion and impregnation challenges, but it allows for manufacturing of complex shapes and the fiber volume fraction is adaptable [47].

The thermoplastic in this project is called polyethylene terephthalate glycol (PETG). The material is chosen because of excellent layer adhesion, thermoforming and low cost [48]. Furthermore, the authors claim it is a durable material with chemical resistance, low moisture absorption, low odour emission and features excellent strength in combination with flexibility.

2.4.4 Limitations and Typical Print Failures

In this section a small selection of printing defects is discussed accompanied with their causes and possible solutions. This can help with increasing the printing quality of the part manufactured in this study.

Warping

In the additive manufacturing process the molten thermoplastic is deposited on a (heated) bed. When this thermoplastic cools down, it can cause warping at the corners due to the internal stresses [49] as illustrated in fig. 2.15. Alsoufi and Elsayed [49] suggest that establishing the correct nozzle and bed temperature reduces warping deformation significantly. If not handled correctly, warping causes printing failures and bad surface quality. Usually, it gets worse with increasing layer deposition due to the pulling force of every single layer [50]. Not only temperature changes solve it, but applying a special adhesion also reduces the chance of warping of the part.

Stringing

Stringing or oozing is caused by overheating the material and happens during non-printing movement of the extruder head [51]. Fig. 2.16 shows a typical example of oozing with the thin strings of polymer that are left behind between the gaps. The effect is reduced by lowering the extruder temperature or increasing the retraction of the filament during non-printing movement [52].

[7] https://unic-3d.com/en/3D-filament-SLA-resin/313-anisoprint-ccf-15k-750m-composite-carbon-fiber.html

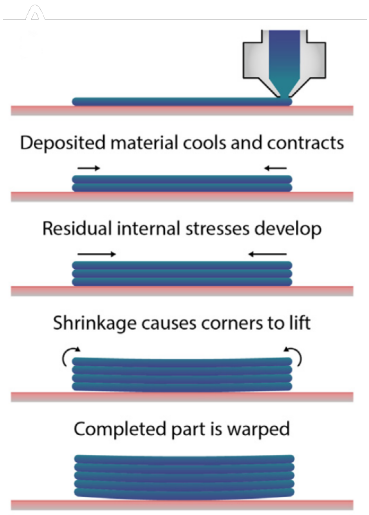

Figure 2.15: Graphic showing the formation of warping in the extrusion 3D printing process [50]

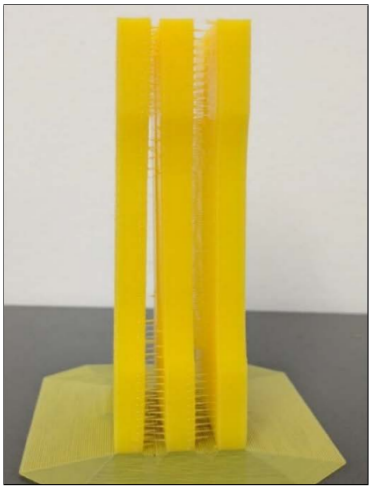

Figure 2.16: Example of stringing in a part manufactured through 3D printing [52]

Layer Defects

Different layer issues exist e.g. separated, misaligned, or missing layers. These problems are often caused by a temperature that is too high or printing speed that is too fast [53]. For instance if a part cools too quickly, it is difficult for the next layer to bond to the already existing print. In this case separation of the layers takes place which results in a faulty part. Shifting of layers is possible when the XY offset is not calibrated properly, since the printer features a dual nozzle system as described in section 2.4.1. Another possible solution is to calibrate the printer accurately before starting to print.

Nozzle Defects

The last common defect is related to the nozzle(s) of the printer. As mentioned before, it is essential to ensure the printer is calibrated; if the nozzle is too close to the part it touches and damages the part whereas when the nozzle is too far from the printing bed the adhesion properties reduce which results in separation of layers. Proper cleaning is necessary to establish a clean (fiber) nozzle. Otherwise, it results in the filament getting stuck in the extruder and not being printed which eventually damages the machine.

Limitations of CFC

The printer that is utilized in this project for the manufacturing of the specimens has a number of limitations and challenges to it. First of all, there is a minimum length for the carbon fibre to be deposited. This is caused by the distance between the cutter and the nozzle. I.e. when the printer cuts the carbon fibre the length of the cutter to the extruder is deposited on the bed, this is the minimum length. A part which perimeter is approximately smaller than 45 mm is not reinforced. Another limitation of the machine is the printing time. The extrusion through the composite nozzle has been experienced as slow. The reason for this extraction rate is to ensure proper impregnation of the carbon fibre with the thermoplastic. Furthermore, the printer only features sensors for in-situ temperature sensing of the extruders and the printing bed. Therefore, most issues that are present on other printers still persist (warping, filament run-out) [54]. With the printer running overnight without in-situ monitoring increases the chance of finding a broken part next morning with filament waste as a result.

2.5 Summary

The Flying V is an aircraft where the fuselage and wing are manufactured out of the same part. Within structural design of aircraft components a grid structure is used to distribute the loads accordingly in the part. The best design for composites is the isogrid structure, since the loads is distributed along all ribs while remaining a low weight. Conventional manufacturing methods for isogrid structures are automated fiber placement (AFP), automated tape layup (ATL), and robotic filament winding. However, the disadvantage is that three times as much fiber builds up in the nodal points if continuous fibers are required in all ribs. Therefore, the chosen strategy is often to cut the fibers before the nodal point or to create an offset where not all ribs run through the same point.

Additive manufacturing is a relative new technology which focuses on producing parts layer by layer. The production of composites has also been made possible through different techniques. The chosen printer in this project is the Anisoprint Composer A4 which features a dual nozzle system for the composite-thermoplastic and thermoplastic. Through this new manufacturing equipment it is possible to have continuous fibers run through all ribs while maintaining an even thickness throughout the part.

3 Materials and Methods

In this section the materials and methods of the project are described. In this project a structure is designed and produced through AM with focus on the nodal point. One advantage of using CFC is that continuous fibers are possible in all individual ribs. The hypothesis is that this increases the mechanical performance of grid structures. This is proved through executing quasi-static tests on the structure. Through these methods the concept of CFC is shown for grid structures in aviation. Mainly two methods are utilized in this project; literature review and experimental work.

3.1 Methodology

Arbnor and Bjerke [55] define three methodological views in their book: the *analytical*, the *systems*, and the *actors* view. The authors argue it is essential to choose a methodology to further understand the context in which a study is placed. The analytical view is focused on generating knowledge or rules through verifying it against data, often seeking for cause-effect relationships. The researcher aims to describe facts they see, make a prediction based on the theory and tries to verify this with facts again. It is a typical method used in science. The systems view is based on the belief that one can only study the system as a whole without separating the sub-components. In order to understand the system it is necessary to analyze the complexity of the system as a whole. The actors view aims to understand reality by integrating in a social construction. Furthermore, it is assumed that the actor's objectivity in this study is impossible to achieve. The actions executed by the knowledge creator influences the outcome of the environment that is studied.

In this project the analytical view is chosen. The focus is purely on the mechanical performance of a new manufacturing technology and this study aims to prove the concept of this technique. It creates a new strategy for nodal points and expects additive manufacturing to improve the mechanical properties of the structure. If it is concluded that the mechanical properties of a grid structure benefit significantly from the addition of continuous fibers to a thermoplastic, further research focuses on integrating it in a manufacturing system. Currently, the scope is on the relative differences in material properties of different materials. Experiments are executed and specimens are compared to try to draw a conclusion on improvements. The study does not consider surface quality or other mechanical properties other than tensile strength. The manufacturability of the part is based on the improvement in material strength and printing time, not the costs. However, some suggestions are made on what is necessary to achieve manufacturability on a larger scale.

First, a theoretical background is described based on literature to understand how this study related to previous studies and to describe the technique used in this thesis. This supports answering some research questions. A design is created to represent a nodal structure that is repeatedly printed with different configurations. A simulation is created to verify the behaviour of the structure during testing. When it comes to the data acquisition it is based on *quantitative* research. The numbers on the mechanical strength are generated by executing experimental work [56]. However, there is a *qualitative* analysis on the results of the CT scan. Fig. 3.1 illustrates a summary of the system description as described above.

3.2 Literature Review

In order to understand the topic to its full extent the theory was separated into different sections. First, general knowledge related to additive manufacturing was studied with a focus on FDM. Further investigations elaborated on the different techniques to produce composites through layer-by-layer manufacturing. Through this theory, it is possible to distinguish the technology and elaborate on the

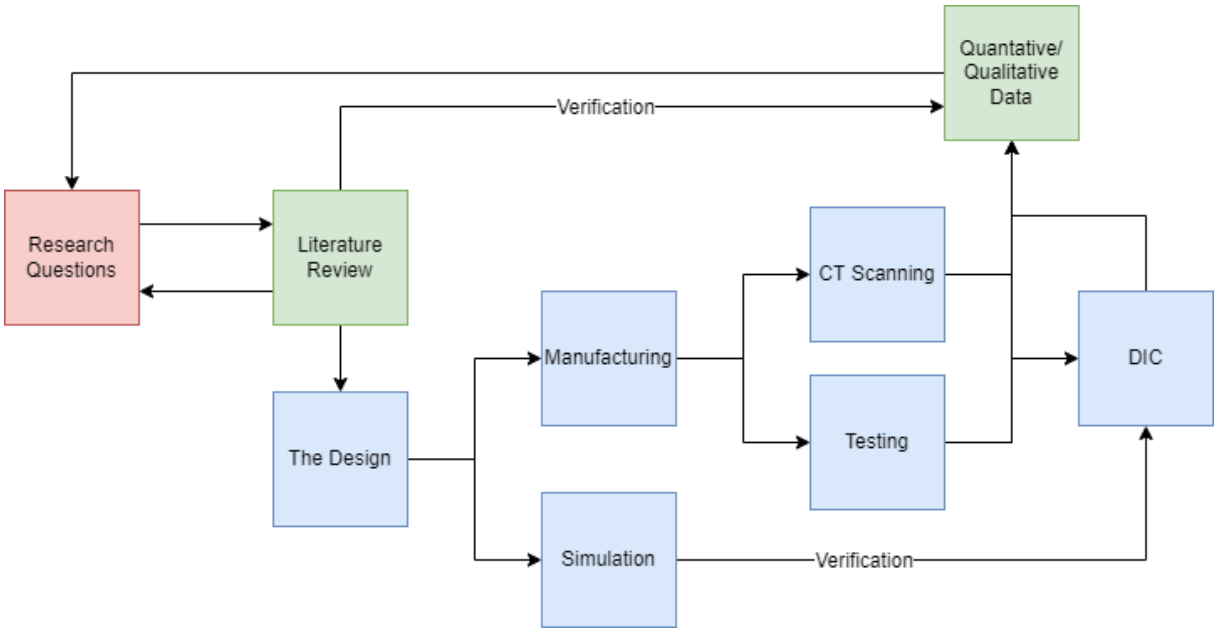

Figure 3.1: System Description

differences and similarities with existing manufacturing techniques.

The Flying V was accurately studied through literature to get a deeper understanding of what greater level the project contributes to. Fig. 3.2 shows an illustration of the pyramid of testing which is often followed in aerospace applications [57]. Currently, the project is at the coupon level but the outcome can be used at a higher stage of the pyramid to forecast the behavior of larger components.

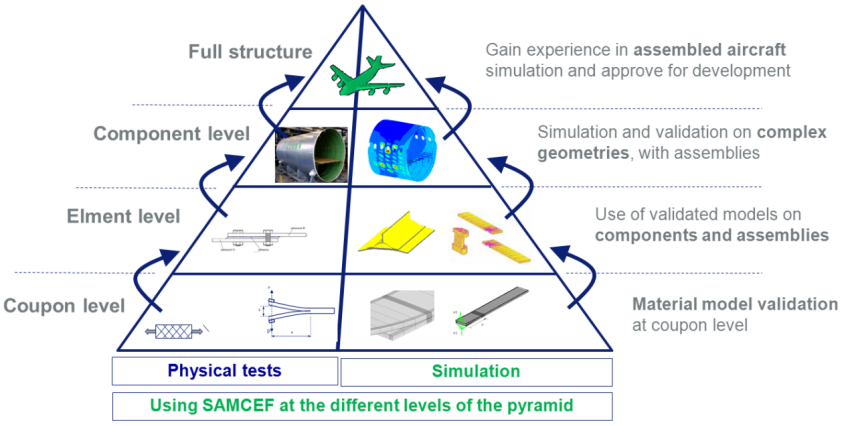

Figure 3.2: Pyramid of testing [57]

Isogrid structures are studied related to their current manufacturing technologies and behaviour. The challenges and advantages of these structures were investigated to see what possibilities the composer A4 offers to composite lattice structures.

3.3 Experimental Work

In this section the different steps are described which are taken to receive the outcome discussed in chapter 4. First, it is argued why this design was chosen. Thereafter, the manufacturing steps and parameters are described. In the end, the tests and equipment are written.

3.3.1 The Design

An accurate representation of an isogrid structure is necessary for the reliability of this project. A typical grid structure is shown in fig. 2.1. The first design is displayed in fig. 3.3a. This structure has different nodal points with ribs coming in from multiple directions. However, it makes the experimenting complex and has several duplicate nodes. Although the second design in fig. 3.3b offers less complexity, the thickness of the grid on top of the skin creates an extra factor in testing. The structure in fig. 3.3c does not have this issue, but the bars on the side reduce the stress on the nodal point. Fig. 3.3d is the design that is created based on the problems described above.

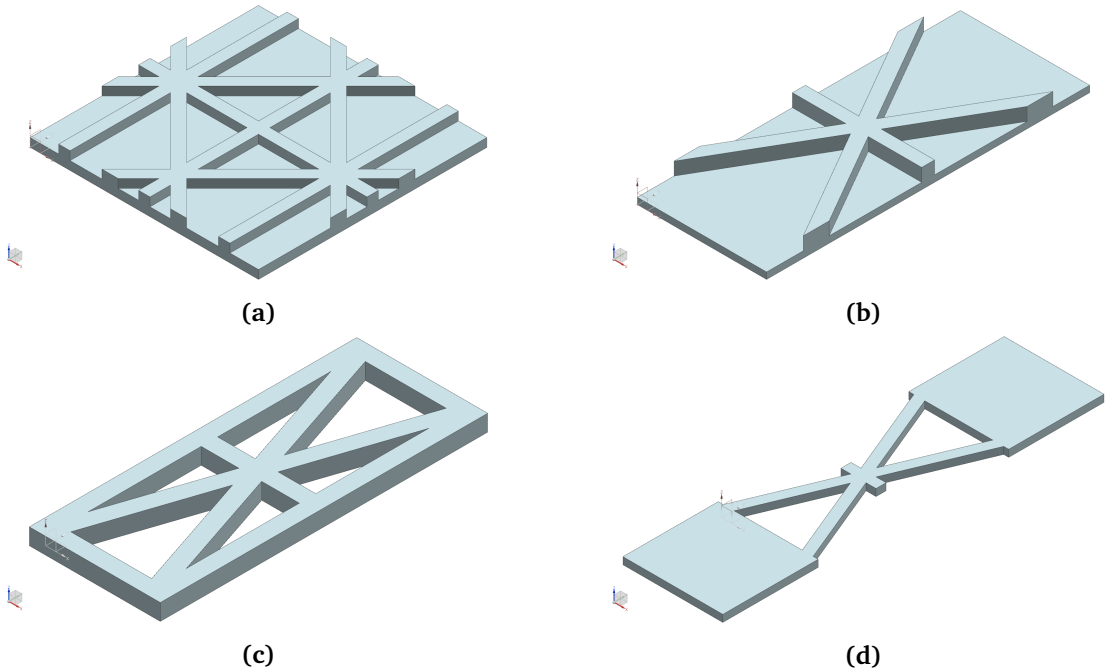

Figure 3.3: (a) First, (b) second, (c) third, and (d) fourth design concept for the structure

Three different designs are tested with changing angles between two ribs of 30°, 45°, and 60° as shown in fig. 3.4. The most important dimensions are visualized in fig. 3.5. The width of the tabs change with different angles. The thickness of 3.5 *mm* for the tabs is accurately chosen to fit the Instron machine that is used for testing.

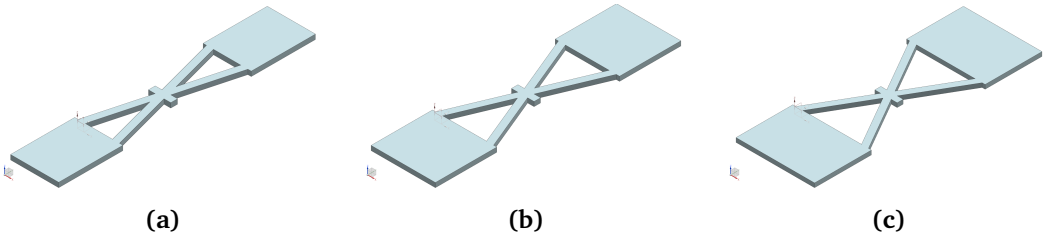

Figure 3.4: Node with (a) 30 °, (b) 45 °, and (c) 60 °rib angle

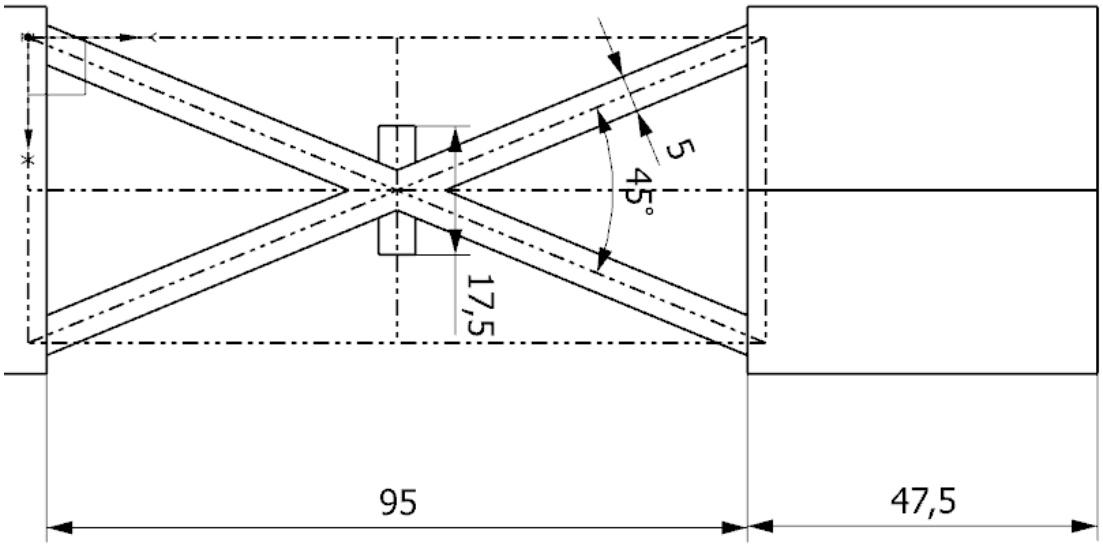

Figure 3.5: Dimensions of the specimen

3.3.2 Manufacturing

The Anisoprint Composer A4 is used in this project to manufacture the specimens. The printer uses a dual nozzle setup as described in section 2.4.1 that reaches temperatures up to 270 °C. Other features include a printing bed that can be heated up to 120 °C and an enclosed chamber to maintain the optimal temperature. The slicer software that is used for printing the composite structures is called Aura and is discussed later. Fig. 3.6 shows a visualization of the printer[1].

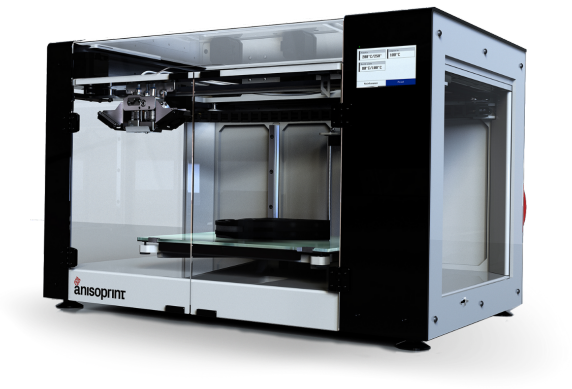

Figure 3.6: Anisoprint Composer A4

[1] https://www.aniwaa.com/product/3d-printers/anisoprint-composer/

Prototype on Prusa Printer

The first prototype is produced on the Prusa i3 MK3S+ printer with polyethylene terephthalate glycol (PETG) filament through fused deposition modeling (FDM). These prints are produced to determine the quality of the design. Four initial structures are manufactured with a length from top to bottom of respectively: 25 *mm*, 50 *mm*, 100 *mm*, and 150 *mm* and are displayed in appendix A.1. PETG is used because of its properties and relevance to composites; it is strong, has low shrinkage properties, not brittle and layer adhesion is excellent [58]. The parameters chosen for the printing are shown in table 3.1.

Table 3.1: Parameters used on Prusa printer for prototype manufacturing

Parameter	Dimension
Infill	60%
Infill pattern	Concentric
Brim width	5 mm
Filament diameter	1.75 mm
Layer height	0.20 mm
Nozzle temperature	240 °C - 250 °C
Bed temperature	85 °C - 90 °C

It was discovered that the specimens with length smaller than 5 *mm* experienced warping and bad surface quality. The larger samples have excellent surface quality and no visible defects. Therefore, a length of around 100 *mm* is chosen for the final specimen.

Manufacturing

Additive manufacturing consists of a set of steps; first, the CAD file is exported from Siemens NX to an .STL file that is read by the Aura software. Within the Aura software the printing profile of CFC and PETG is chosen with no adaptions to the printing parameters. A plastic infill of 45% is used with the isogrid pattern. Two different specimens are manufactured for each angle, one with two reinforced fibers shells along the perimeters and one fabricated using purely PETG. An example is provided in fig. 3.7 where the bright blue lines represent the fibers and the green lines represent pure plastic. All the important parameters are summarized in table 3.2. Besides these parameters the standard settings for the Clear PETG / CCF 1.5k + Clear PETG are used as this profile turned out to be the best fit after observation. The sliced file is exported to an SD card as gcode which is read and executed by the composer A4 to produce the desired part.

Table 3.2: Most important parameters

Parameter	Reinforced Specimen	Non-Reinforced Specimen
Infill	45%	45%
Infill pattern	Isogrid	Isogrid
Reinforced Perimeters	2	0
Brim	10 loops	10 loops
Marcolayer height	0.34 mm	0.17 mm
Other layers height	0.17 mm	0.17 mm
First layer height	0.2 mm	0.2 mm
Extruder temperature	235 °C	235 °C
Build plate temperature	80 °C	80 °C

The CFC printer is located in a dedicated room with dry climate and optimal temperature for the filament not to get humid. For the reinforcement, continuous carbon-epoxy filament is used which contains 1500 carbon fibres. The material features an elastic modulus of 149 GPa, a tensile strength of 2206 MPa, and a carbon fibre volume fraction of 60% [59]. As discussed in section 2.4.3, the filament is impregnated with a special thermoset matrix. For the thermoplastic matrix PETG is chosen due the adhesion performance with the carbon fibre filament [59]. To ensure dry filament, the PETG was dried in the oven at 65 °C for four to six hours. To increase adhesion between the glass build plate and the printed part, Magigoo is used that acts as a glue between the part and the bed. Before manufacturing is started, all necessary calibration steps are executed to reduce the risks of print imperfections.

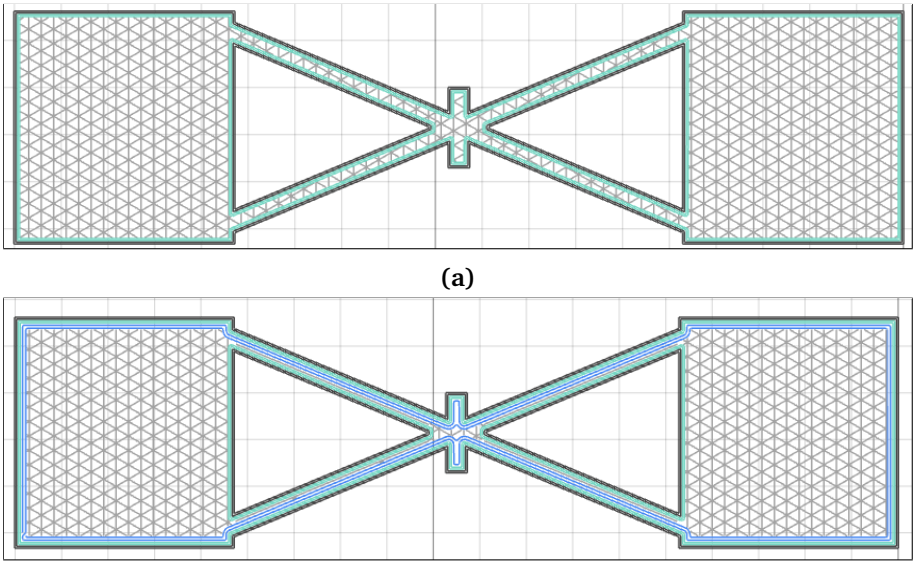

(a)

(b)

Figure 3.7: (a) Non-reinforced specimen and (b) reinforced specimen as defined in Aura

After manufacturing of the specimens the tabs are processed with sand paper and glass fibre reinforced epoxy is cut to the size of the tabs. The glass fibre and tabs are bonded together with a super glue adhesive and the end results is shown in fig. 3.8. These tabs are used to increase friction between the tabs and the grips of the Instron testing machine.

Figure 3.8: Specimen with glass fibre tabs attached

3.3.3 Testing Setup

In this section the testing equipment and parameters are described that are used in this thesis. There is the Instron machine, the DIC, and the CT scan. The next section focuses on the data processing for the creation of the results.

Instron 5966 UTS

Tensile tests are carried out to analyze the structural performance of the specimen. The test is executed at room temperature using the Instron 5966 UTS machine with a load cell of 10 kN. The samples are prepared as described above and are tested with a displacement rate of 2 mm/min. Two white dots are placed on both ends of the node to measure the strain with the extensometer attached to the Instron machine as shown in fig. 3.9a. The tabs at both ends are secured in the middle of the grip with a pressure of around 4 bars to not cause failure in the tabs.

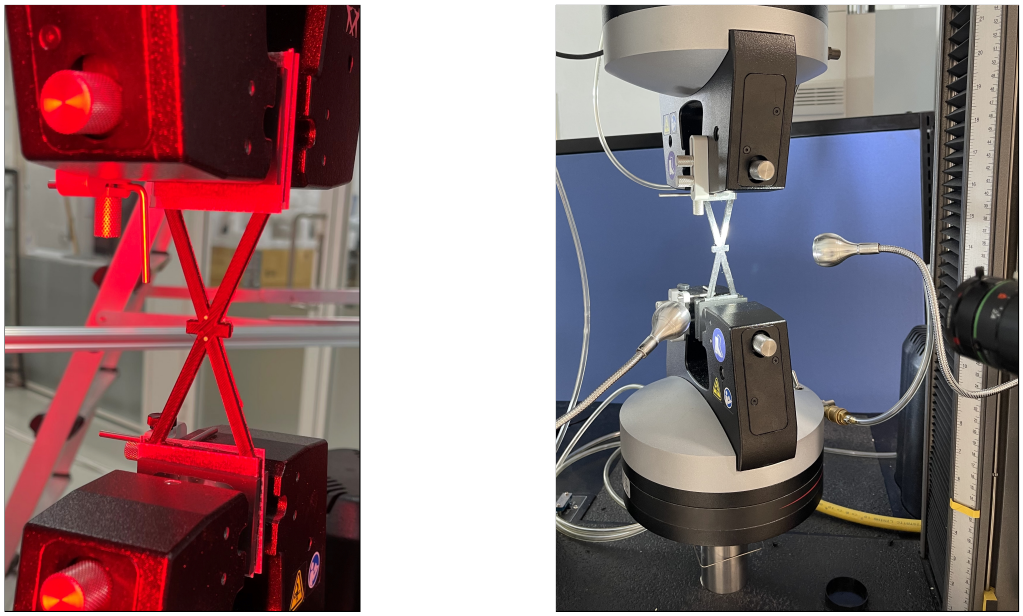

(a) **(b)**

Figure 3.9: (a) Specimen prepared for extensometer and for (b) DIC strain mapping

Digital Image Correlation

Digital Image Correlation is a full-field image analysis method coupled with the Instron machine to measure strains to the point of proportionality. In this project, it is used for strain mapping of the whole structure. The DIC system uses a Teledyne DALSA 7 MP camera capable of 62 fps, with an operating temperature varying from -20 °C to 145 °C. The software package is VIC-2D from correlated solutions. In this process, the camera is first calibrated by using a speckle pattern designed for the camera system. This helps to create an accurate and sharp image of the object to be tested. A neutral background behind the specimen as well as tweaking the focus and brightness ensures a high quality result. The pictures are taken at a rate of 1 Hz to correlate it to the stress-strain curve created by the testing machine. Fig. 3.9b displays the full setup including the lights.

CT Scan

Small errors in aircraft components components made with composites lead to a significant reduction of the structural performance [60]. Therefore, it is essential to ensure that such defects are not present in the manufactured part. One method of non-destructive analysis of composites is x-ray computed micro-tomography (CT). This evaluation method is based on the reconstruction of radiographs that are obtained by applying different angles of illumination [61]. In this thesis, the CT scan is used to check the fiber orientation in the node. One section of a rib is analyzed to determine how many fibers are in the direction of the rib. Furthermore, the part is scanned to check for small printing defects. This is used to evaluate the manufacturing quality.

3.3.4 Data Acquisition

The parameters acquired through the tensile test are the force applied by the loading cell, the tensile strain measured by the extensometer, and the displacement between the upper and lower grip of the Instron machine. A typical stress-strain curve is shown in fig. 3.10. Through eq. 3.1 the stress is calculated in MPa.

$$\sigma = \frac{F}{A_0} \tag{3.1}$$

Where σ represents the stress in MPa, F is the force in N, and A_0 equals the cross sectional area in mm^2 at $t = 0$. The cross sectional area is measured at the nodal point in terms of width times thickness. The strain is calculated through eq. 3.2.

$$\epsilon = \frac{\Delta L}{L} \tag{3.2}$$

Where ϵ represents the strain, ΔL is the distance in length between L_0 and L_t, and L stands for the length at $t = 0$. The Ultimate Tensile Strength is determined through the analysis of graphs created with the outcome of the tests as shown in area C in fig. 3.10. The equation for the UTS is shown in eq. 3.3.

$$\sigma_{max} = \frac{F_{max}}{A_0} \tag{3.3}$$

In order to determine the fiber volume fraction (V_f) of the specimen eq. 3.4 is used [62] according to ASTM D2584. In this formula ρ_m represents the density of the matrix, ρ_f the density of the fibers, w_m the weight of the matrix and w_f the weight of the fibers. In the calculation of V_f the weight of the tabs is not included as this does not influence the mechanical properties of the specimen.

$$V_f = \frac{\rho_m \cdot w_f}{\rho_m \cdot w_f + \rho_f \cdot w_m} \tag{3.4}$$

3.3.5 Simulation

Initial simulation is executed to verify the behavior of the structure and investigate the stress flow in Siemens NX. A load of 1 N is applied at the top in positive y-direction while the bottom remains fixed. This simulation resembles a tensile test. The result of this simulation is compared to the result of the DIC to verify the mechanical behavior of the specimen and to see if it is as expected. For meshing, a size of 1 mm is chosen for a detailed result. Due to the time limitation of this project the simulation of continuous fibers is not possible and too complex.

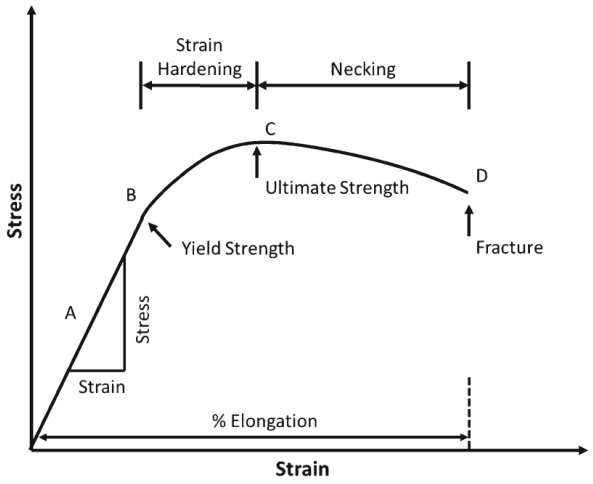

Figure 3.10: Typical stress-strain curve caused by tensile testing [63]

4 | Results and Discussion

In this section the results of the different experiments and scans are shown and it is discussed whether additive manufacturing improves the production of isogrid structures.

4.1 Manufacturing Quality

This section elaborates on the quality of the end product and the overall printing process. For the first specimens it was observed that warping occurred in the same area consistently of the build plate as displayed in fig. 4.1a. The warping was eliminated after accurate calibration of the printer according to the supplier's instructions. Furthermore, the first spool of PETG used was shelved for a long time and contained moisture. Therefore, it was dried in the oven as described before to ensure no bubbles are present in the specimen. The surface quality of the end product was excellent, with a matte finish on the top and a shiny finish on the bottom. The fiber lines were according to the slicer file as shown in fig. 4.1b. Loose strings of the thermoplastic material were detected in the beginning (explained in section 2.4.4), but this was eliminated by adjusting the retraction of the filament during non-printing movements. For more in-depth analysis of the quality the CT scan was used as discussed in the next section.

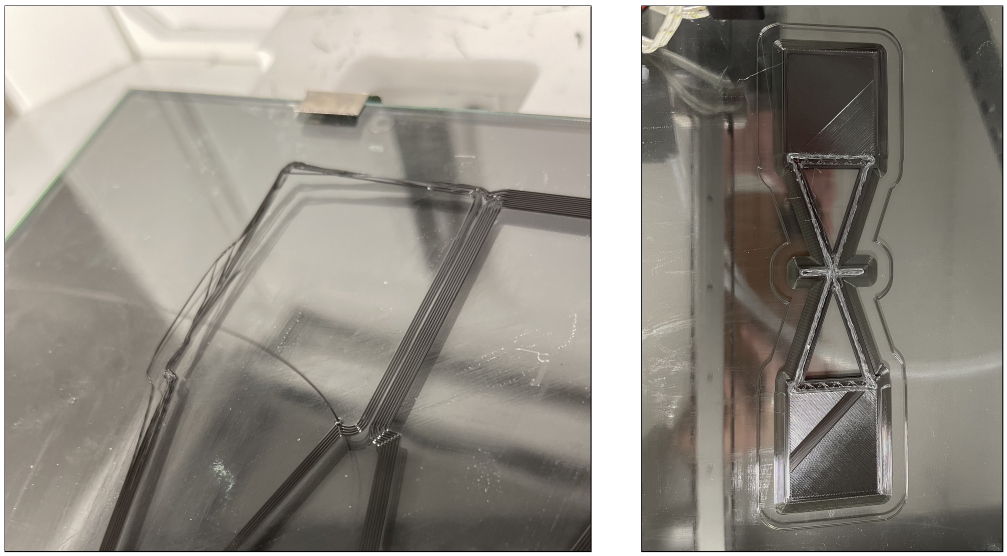

(a) **(b)**

Figure 4.1: (a) Warping of specimen and (b) fiber lines visible during printing

4.1.1 CT Scans

The CT scan is an analysis suitable for detecting defects in part manufactured through 3D printing. Pores and small details that are not seen by the naked eye are seen on the images created by the machinery. In this project it is mainly used to detect printing failures and determine the accuracy by making a comparison with the predicted infill from the slicer software. Therefore, a smaller resolution is chosen that is unfortunately not able to detect pores. However, porosity is a topic already widely investigated for CFC [59, 64]. This is discussed later in more detail.

Non-Reinforced at 30 Degrees

Fig. 4.2a displays the expected printing outcome of one of the inner layers of a non-reinforced specimen at 30 degrees rib angle. Fig. 4.2b is the result of the CT scan of this particular specimen. The isogrid infill pattern is as predicted with the PETG lines crossing one another. However, stringing is detected in particular through the middle and in the bottom right rib. This is internal stringing but has the same cause as external stringing - filament dripping from the nozzle during non-printing movements. Although it does not affect the mechanical behavior of the layer since overall the adhesion is good, it is solved by changing the printing speed or retraction of the filament.

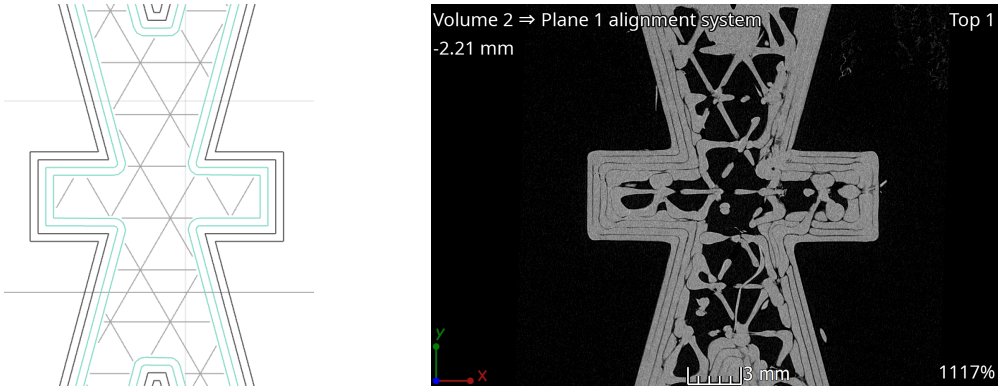

(a) **(b)**

Figure 4.2: (a) Sliced and (b) CT scan of non-reinforced specimen with 30 degrees angle

Reinforced at 30 Degrees

Fig. 4.3a indicates the expected outcome of the infill whereas fig. 4.3b shows the actual outcome from the CT scan of the reinforced specimen manufactured at 30 degrees. There is stringing present in the left part of the node indicated by the broken lines. The fiber lines correspond to the predicted lines provided by the Aura software and appear to be continuous through all ribs. However, the fiber paths seem waivy in the left top part of the specimen.

Within the CT scan software it is possible to run a "fiber-composite analysis". One of the provided outputs of this analysis is the direction of the fibers within the scanned specimen. In this specimen it is desired that the fibers are in the direction of the rib. For this particular specimen it was determined that 95% of the fibers were in the desired orientation. Fig. 4.4b indicates the result of the fiber composite analysis. The green lines indicate in what direction the fibers are pointed. The figure displays one slice of the fiber block displayed as an example. Fig. 4.4a displays the section that is used for the analysis. It is observed that most arrows point in the rib direction with small deviations in other directions. Taken into consideration measurement inaccuracies it is not possible to achieve 100 % in the direction of the rib with this resolution.

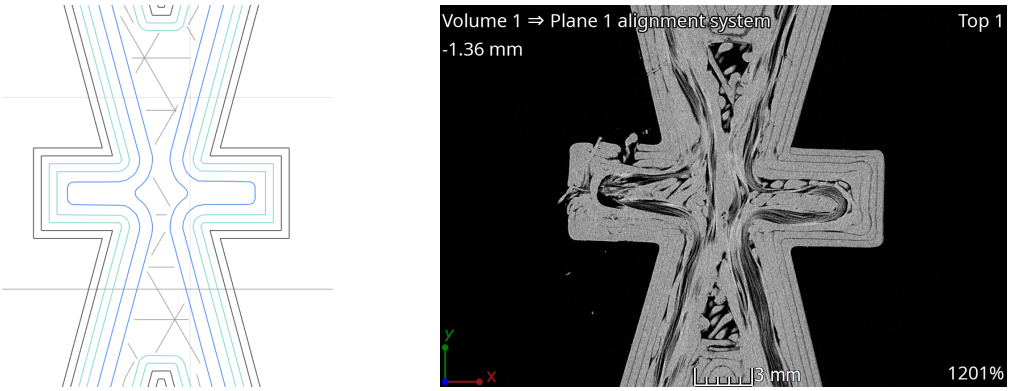

(a) **(b)**

Figure 4.3: (a) Sliced and (b) CT scan of reinforced specimen with 30 degrees angle

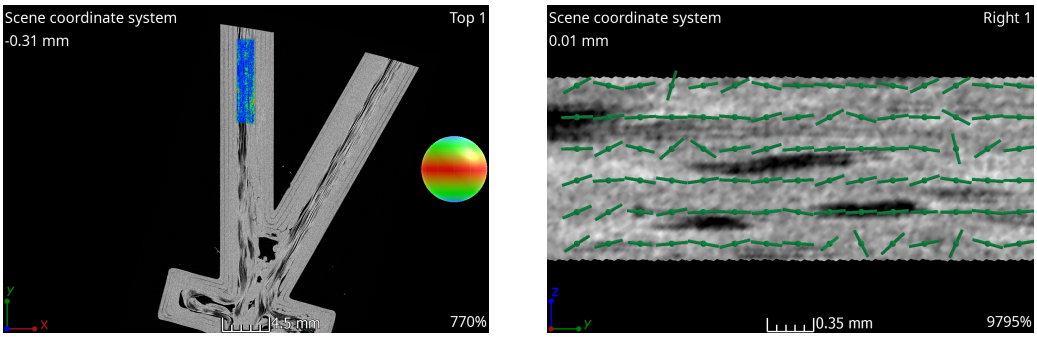

(a) **(b)**

Figure 4.4: (a) Analyzed section and (b) fiber orientation of reinforced specimen with 30 degrees angle

Non-Reinforced and Reinforced at 45 Degrees

Fig. 4.5 and fig. 4.6 represent the images for the configuration at 45 degrees. The same observations are done here. There is small areas with stringing but overall the infill is as expected. The fiber lines are continuous through all ribs as well and there are no visible waivy pattern in the fiber paths. Through the software the fiber orientation was determined as 97% in the direction of the rib.

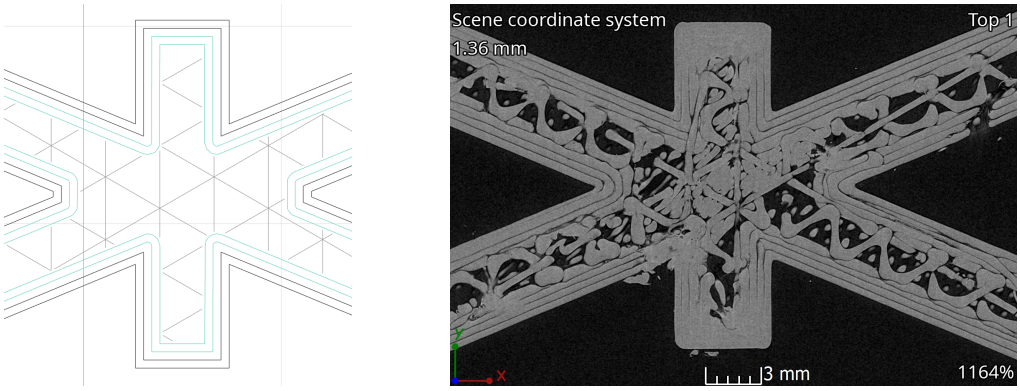

(a) **(b)**

Figure 4.5: (a) Sliced and (b) CT scan of non-reinforced specimen with 45 degrees angle

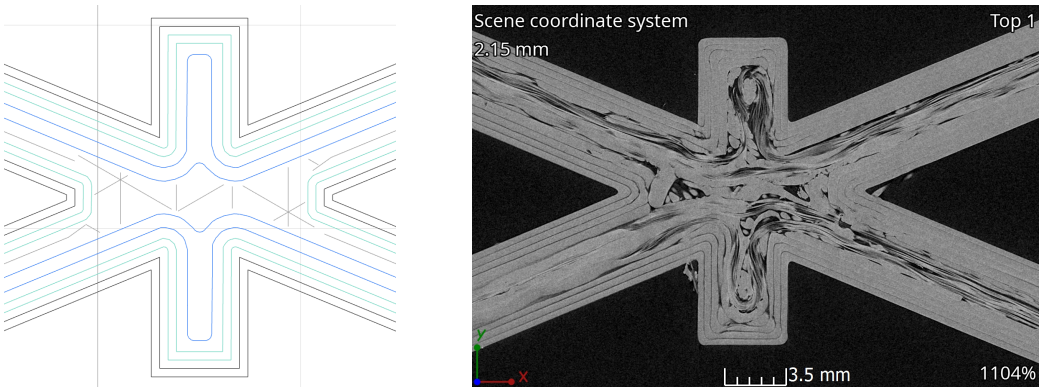

(a) (b)

Figure 4.6: (a) Sliced and (b) CT scan of reinforced specimen with 45 degrees angle

Reinforced at 60 Degrees

Fig. 4.7 displays the reinforced configuration at 60 degrees rib angle. The infill is as expected and is seen through the two fiber lines in the middle of the node. This is also an area of concern since the stress and strain is the highest in the nodal point of the structure - where for this specimen no reinforcement is present. Besides the aforementioned stringing, no other printing defects are detected. Through the software the fiber orientation was determined as 95% in the direction of the rib.

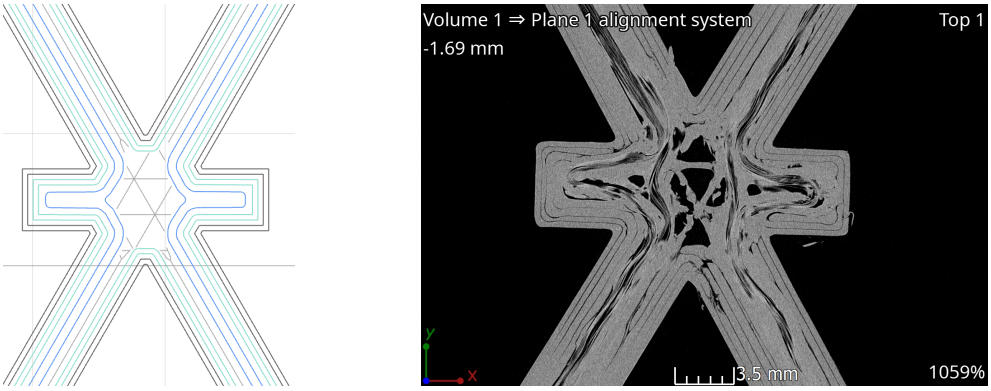

(a) (b)

Figure 4.7: (a) Sliced and (b) CT scan of reinforced specimen with 60 degrees angle

4.1.2 Manufacturing Times

Fig. 4.8 displays the manufacturing times of the different configurations. Between the reinforced and non-reinforced specimen is on average 33 minutes difference. This is caused by the slow deposition time of the fibers onto the printing bed in order to ensure proper adhesion and due to the stiff characteristics of the material. It makes sense that the extra time is almost similar, since the amount of fiber in each specimen is nearly identical. It is important to take manufacturing times in consideration when shifting to industrial scale. More reinforcement usually means a stronger structure at the cost of efficiency - especially in additive manufacturing. Through fig. 4.8 it is concluded that 0.49 grams of CCF takes around half an hour to be manufactured. The increase in printing time when the angle increases is caused by the increase in deposited volume. The tab size increases as well as a small increase in overall surface area in the node.

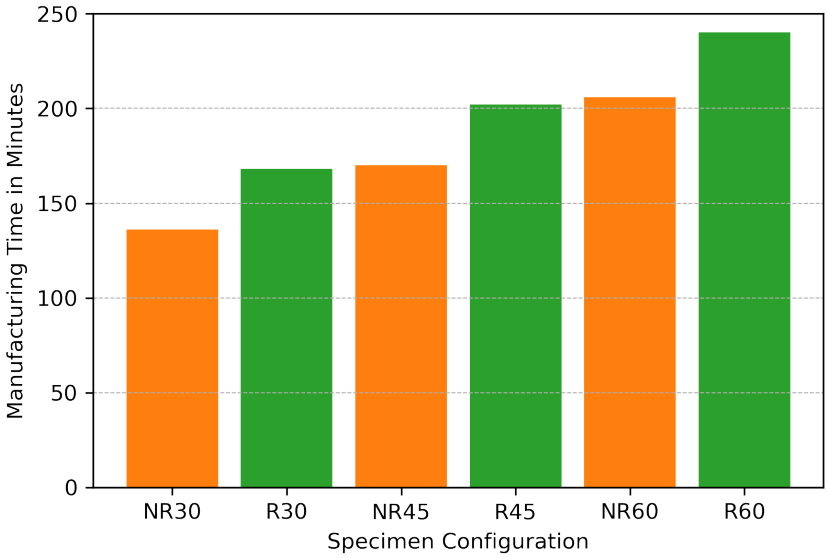

Figure 4.8: Manufacturing times of one specimen with indicated configuration

4.2 Fiber Volume Fraction

It is important to calculate V_f first before elaborating on the results to get an indication to what extent the fibers influence the mechanical properties of the specimen. The formula for the calculation of V_f is shown in eq. 3.4. The carbon fiber filament consists of approximately 70 wt% carbon and 30 wt% epoxy resin [65]. The density for the matrix[1] (ρ_m) is 1.27 g/cm^3 and the density of the fibers (ρ_f) is 1.7 g/cm^3 at room temperature[2]. The different weights are extracted from the Aura Slicer software and displayed below. Note that the slicer software only provides the weight with one decimal, explaining why V_{f45} is significantly lower.

- For the 30 degrees configuration:
  - $w_m = 4.8$ g
  - $w_f = 70\% \cdot 0.7$ g $= 0.49$ g
- For the 45 degrees configuration:
  - $w_m = 5.2$ g
  - $w_f = 70\% \cdot 0.7$ g $= 0.49$ g
- For the 60 degrees configuration:
  - $w_m = 5.4$ g
  - $w_f = 70\% \cdot 0.8$ g $= 0.56$ g

Using this information the different fiber volume is calculated as displayed below.

$$V_{f30} = \frac{1.27 \cdot 0.49}{1.27 \cdot 0.49 + 1.7 \cdot 4.8} = 0.0708 \approx 7.1\%$$

$$V_{f45} = \frac{1.27 \cdot 0.49}{1.27 \cdot 0.49 + 1.7 \cdot 5.2} = 0.0657 \approx 6.6\%$$

$$V_{f60} = \frac{1.27 \cdot 0.56}{1.27 \cdot 0.56 + 1.7 \cdot 5.4} = 0.0719 \approx 7.2\%$$

[1] https://addnorth.com/product/PETG/PETG%20-%201.75mm%20-%202300g%20-%20Black
[2] https://www.chemsrc.com/en/cas/1333-86-4_746695.html

It is difficult to conclude on a number as the desired fiber volume fraction - as it depends on the application for the composite. Furthermore, while the compressive strength increases with increasing V_f to some extent, the in-plane shear strength decreases [66]. Taheri-Behrooz *et al.* [66] determined the optimum fiber volume fraction considering compressive strength and in-plane shear strength and experimentally concluded that 44.6% is the optimal fiber volume fraction. Another study by He and Gao [67] concluded that for uni-directional fibers a range between 50% and 70% is optimal for the fiber volume fraction. Above this number, flexural properties appear to be poor.

The carbon fibre filament has a V_f of 60%. Through (the abovementioned) literature it is concluded that a V_f of at least 40% is required for a high strength/stiffness structure, but in aerospace engineers typically try to achieve up to 60%[3]. The supplier of the filament reports that normally a fiber volume fraction of 45% is achieved with normal use of CFC. However, with their method carbon fibre crosses one another without thickening of the material in contrast to e.g. AFP due to the local pressure increase of the nozzle during printing. Therefore, additive manufacturing has the potential to achieve even higher fiber volume fractions than conventional manufacturing methods for composites.

[3] https://www.engineering.com/story/anisoprint-anisotropy-as-advantage-in-carbon-fiber-3d-printing

4.3 Tensile Tests

The experiments carried out are based on pulling a specimen on both ends. Load is applied until the specimen fails and a typical stress-strain curve is the result. The data from this curve shows different characteristics of a specimen and its material. The stress-strain curve is created based on the load-displacement curve and the cross-sectional area of the node as described in section 3.3.4.

4.3.1 Load-Displacement - 30 Degrees

Fig. 4.9 shows the load-displacement curve for the configuration with 30 degrees. The other load-displacement curves are displayed in appendix A.2. The curve shows linear behaviour as it is based purely on the parameters measured by the machine (linear input). The displacement rate is set at a constant rate of 2 mm/min. It is observed that the reinforced specimens handle significant larger loads before fracture than its non-reinforced equivalent. However, the maximum displacement is higher for the non-reinforced specimens - caused by the stiff fiber bundles inside the specimen.

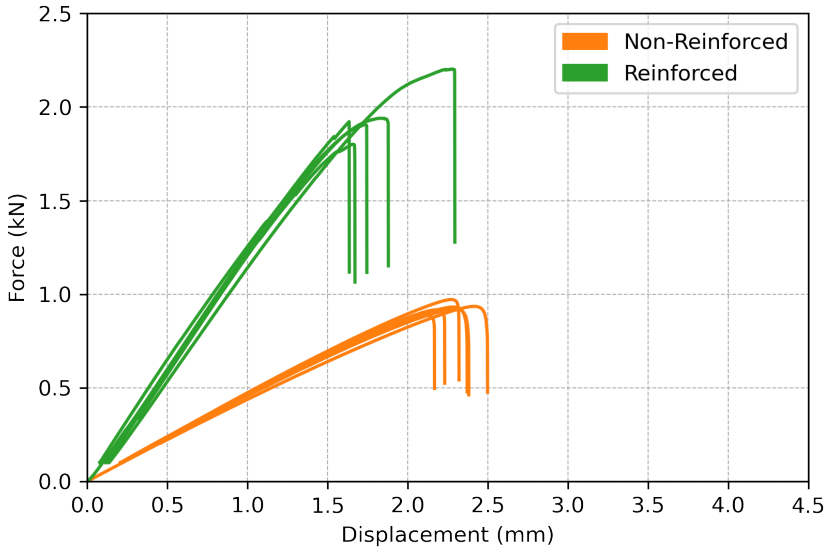

Figure 4.9: Load-displacement curve of nodes with 30 degrees rib angle

4.3.2 Stress-Strain - 30 Degrees

Fig. 4.10 shows the stress-strain curve of the configuration with 30 degrees angle. The so-called vibrating behaviour is caused by the printing lines of the specimen that are diagonal - these are measured by the extensometer.

First of all, it is observed that the reinforced specimens have a higher maximum stress before they fail as well as a lower strain - indicating stronger and stiffer mechanical behaviour - as expected based on the mechanical characteristics of carbon fibre. The fiber is embedded and impregnated with the PETG inside the specimen and ensures an increase in mechanical performance. The specimen appears to fail in the polymer interface since the fibers remain intact. However, the presence of the fibers improve the mechanical performance of the specimen by adding strength to the thermoplastic material. The necking phase for the reinforced specimen is shorter than for the non-reinforced equivalent. This is explained by the brittle behavior of the fiber that impacts the overall behavior of the structure.

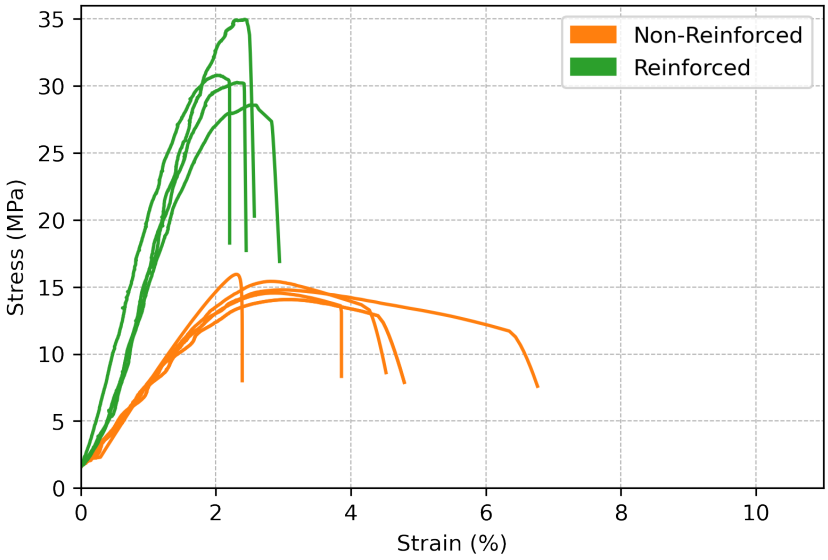

Figure 4.10: Stress-strain curve of nodes with 30 degrees rib angle

4.3.3 Stress-Strain - 45 Degrees

Fig. 4.11 shows the stress-strain curve of the configuration with 45 degrees angle. The corresponding load-displacement curve is displayed in fig. A.2. The same behavior is observed as for the configuration at 30 degrees rib angle. The reinforced specimen has a higher tensile strength before failure whereas the non-reinforced specimen is less brittle. However, the specimens are less stiff than the specimen manufactured with a 30 degrees rib angle because of the increase in area due to the larger angle. This is also seen through the maximum strain that appears to be significantly higher compared to the 30 degree configuration.

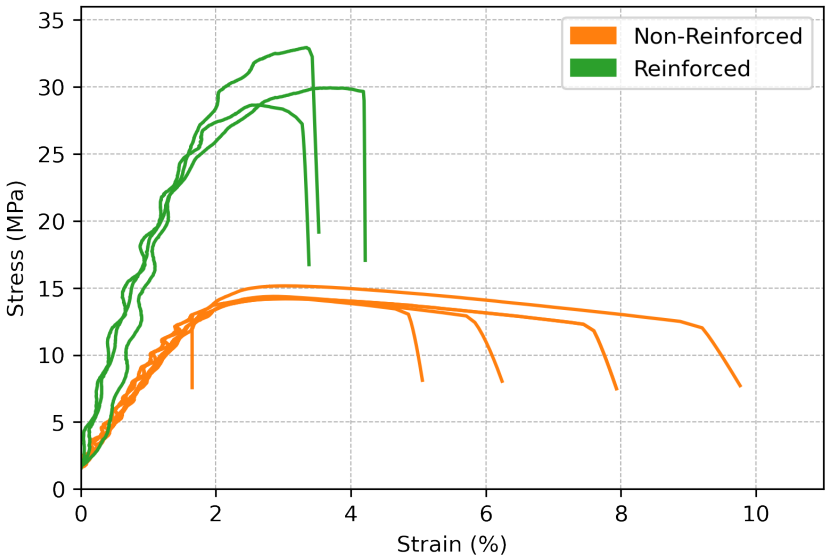

Figure 4.11: Stress-strain curve of nodes with 45 degrees rib angle

4.3.4 Stress-Strain - 60 Degrees

Fig. 4.12 shows the result of the tests executed on the specimen with 60 degrees rib angle. The behavior is similar to the previous configuration of 45 degrees. Due to the increase in area the specimen appears to be more elastic and there is a small increase in maximum strain. The configuration showed different failure behavior than the other specimens, but this is discussed in section 4.3.5.

Table 4.1 represents the mean and standard deviation of the maximum stress and strain of all the specimens. It is concluded that after the maximum value has been reached the specimen fails. From this table it is observed that a reinforced specimen is approximately two times stronger than a non-reinforced specimen with less than 10% of fiber volume fraction (see section 4.2). Furthermore, the mean values of both the reinforced configurations and the non-reinforced configurations are relatively close - with only one reinforced 60 degrees specimen being significantly lower than the rest (causing the high standard deviation). The similarity between the specimens is confirmed by fig. 4.13 and fig. 4.14 where the graphs are all closely related on another.

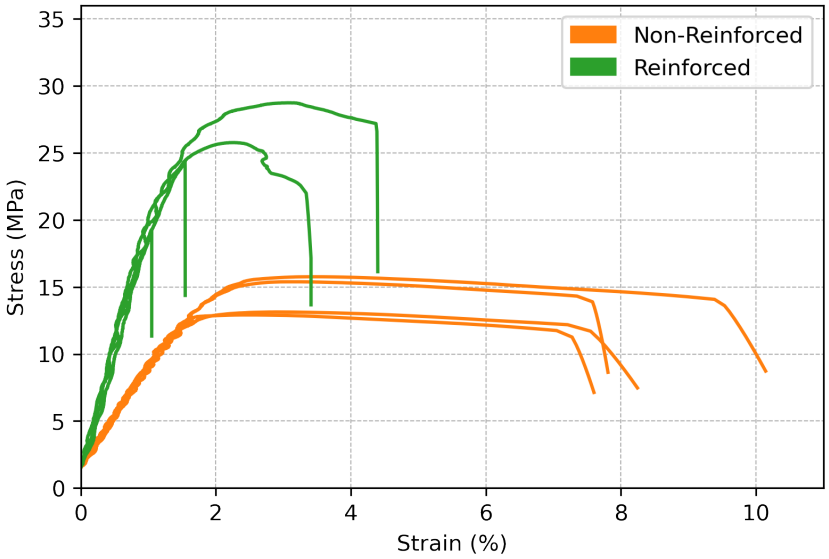

Figure 4.12: Stress-strain curve of nodes with 60 degrees rib angle

Table 4.1: Mean and standard deviation of stress and strain of the tested specimens

	Stress [MPa]	σ	**Strain [%]**	σ
NR30	15.00	0.67	2.75	0.29
R30	31.20	2.34	2.19	0.35
NR45	14.29	0.75	2.69	0.52
R45	30.47	1.80	2.89	0.81
NR60	14.55	1.40	3.16	0.55
R60	25.53	4.05	2.11	0.81

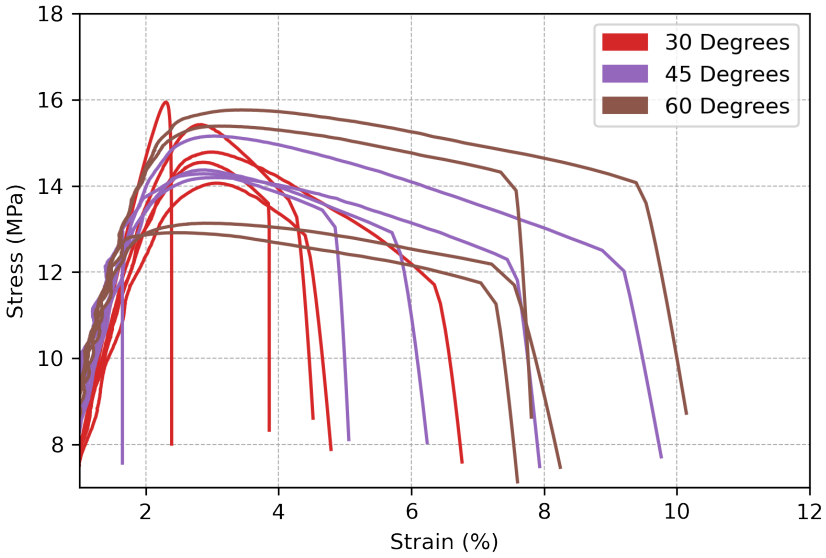

Figure 4.13: Stress-strain curve of non-reinforced nodes

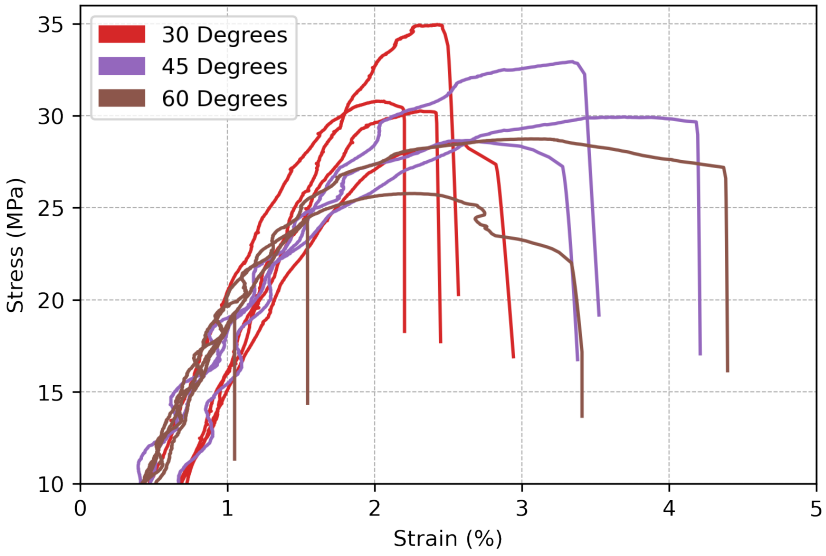

Figure 4.14: Stress-strain curve of reinforced nodes

4.3.5 Failure Modes

The fracture that occur after testing are studied to analyze the behavior. Furthermore, odd cases are discussed more in-depth to determine their cause and meaning.

Fig. 4.15, fig. 4.17 and fig. 4.18 all indicate different failure outcomes of the tensile test. PETG is described as one of the more ductile filaments[4]. This is observed in fig. 4.15a where there is small deformation present after complete separation of the top and bottom of the specimen.

For the reinforced specimen (fig. 4.15b) it is observed that after failure it is difficult to discover deformation, indicating a more brittle fracture mode than its non-reinforced equivalent (however, local plastic deformation is present). It is concluded that this is caused by the addition of the carbon fibre filament - having brittle behavior. This corresponds to the stress-strain curves displayed in section 4.3 where there is a sudden failure of the specimen after the maximum load is reached.

Fig. 4.15a and fig. 4.15b show the fracture mode that represent 19 out of 25 specimens where fracture occurs in the middle of the node. The crack in the middle is nearly perpendicular to the direction of the stress. Interesting to mention is that the specimens did not crack through a printing line. The location of the crack occurs independent on the presence of reinforcement. Furthermore, the fiber remains intact and does not separate completely due to its strong tensile properties. Specifically, the filament has a tensile strength of 2206 MPa.

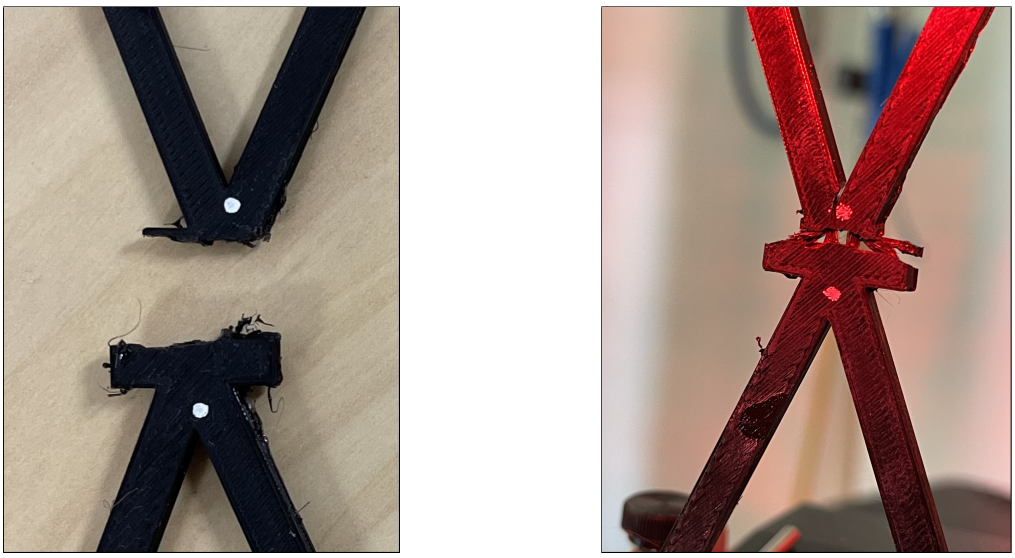

(a) **(b)**

Figure 4.15: Failure mode of (a) non-reinforced and (b) reinforced specimen with 45 degrees rib angle

[4] https://prusament.com/materials/prusament-petg/

To confirm the specimen indeed failed another tensile test was executed after failure of the PETG with the fiber intact through the top-bottom separation. No increase in stress-strain curve is observed. It is concluded that the carbon fibre gets its strength from the PETG it is impregnated in. Fig. 4.16 shows an in-situ image while executing the test described above. There is complete separation of the bottom ribs and there seems to be loose fiber fragments present that disconnected from the large fibre bundles.

Figure 4.16: Applying stress after failure on reinforced specimen with 45 degrees rib angle

For the specimens at 60 degrees it is observed that failure often occurs in the ribs in contrast to the middle of the node. 4 out of 10 specimens either failed along the rib as displayed in fig. 4.17b or had a complete separation of one of the ribs as displayed in fig. 4.17a. An explanation for this failure is the large empty space within the node as discussed in section 4.1.1. There is no separation of the top and bottom part in the reinforced specimen as displayed in fig. 4.17b.

(a)

(b)

Figure 4.17: Failure mode of (a) non-reinforced and (b) reinforced specimen with 60 degrees rib angle

One of the reinforced specimens with a 30 degrees rib angle features a complete fracture through the middle of the node as visualized in fig. 4.18. The fracture occurs parallel to the stress instead of perpendicular. One cause can be the absence of continuous fibers from the left of the specimen to the right. However, none of the other nodes feature a fracture in the direction of the load. Although it is known that composites typically fail in different ways and it is more difficult to predict their behavior. Nonetheless, is this particular fracture parallel to the direction of the stress not logical in a standard tensile test.

Figure 4.18: Failure mode of reinforced specimen with 30 degree rib angle

4.3.6 Tensile Tests - DIC Strain Mapping & Simulation

For each configuration a DIC is taken during the tensile test to analyze the mechanical behavior of the whole specimen. The figures displayed on the following pages all demonstrate how strain localization is formed inside the sample. ϵ_{yy} was observed to be the most prominent and therefore analyzed. The last DIC snapshot in each graph is taken right before failure. The dark blue color features a strain of -2% whereas the red stand for a strain of 10%. The DIC results correspond to the results from the other tensile tests with strain mapping using the extensometer. The strain inside the non-reinforced specimen gets significantly higher than in the reinforced specimen. The local strain is the highest in the nodal point where fracture occurs as described in section 4.3.5. In this area, the strain gets as high as 10% for the non-reinforced specimen. Through the DIC the odd failure modes cannot be explained as the images all follow the same behavior.

Fig. 4.19 displays the result of the simulation of the specimen with 30 degrees rib angle. The other simulation results are similar and displayed in appendix A.4. It is observed that the same pattern is present in the simulation - with higher stress distributed as a cross in the node. This agrees with the information provided in section 4.1.1 - that the middle of the node is the area of concern. It is also concluded that adding continuous fibers through the ribs versus pure plastic does not alter the stress distribution inside the specimen. However, perhaps different fiber distribution enables more stress in different areas.

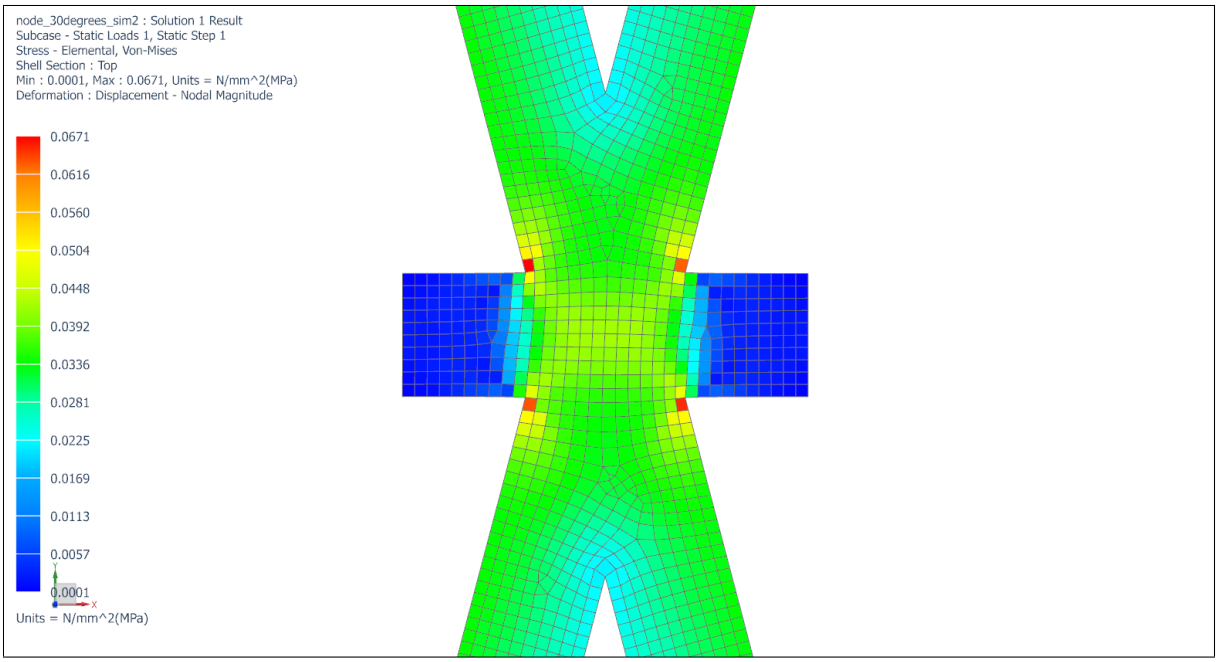

Figure 4.19: Von Mises result of simulation of tensile test with 30 degrees rib configuration

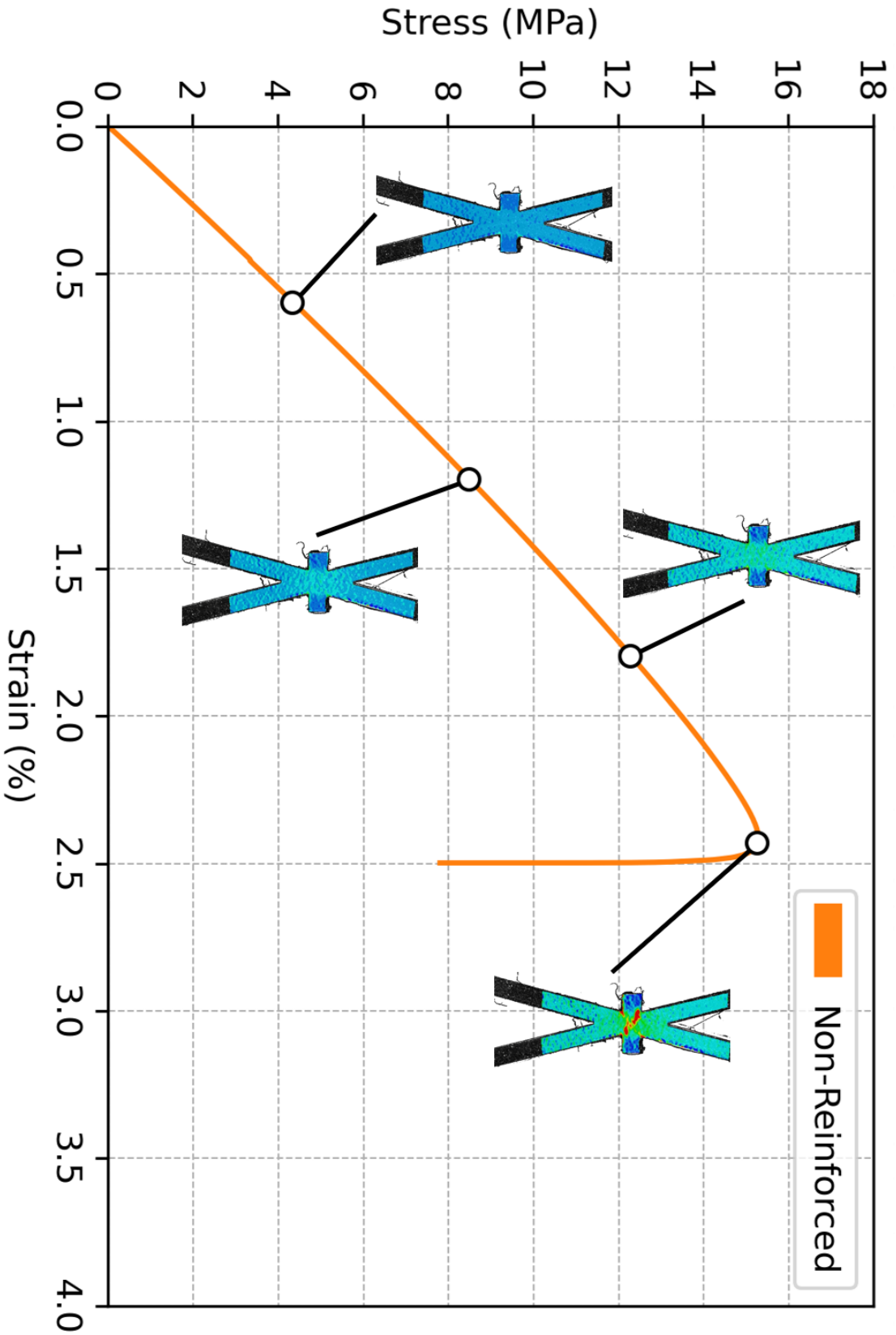

Figure 4.20: Stress-strain curve of non-reinforced node with 30 degrees rib angle and ϵ_{yy} strain mapping using DIC

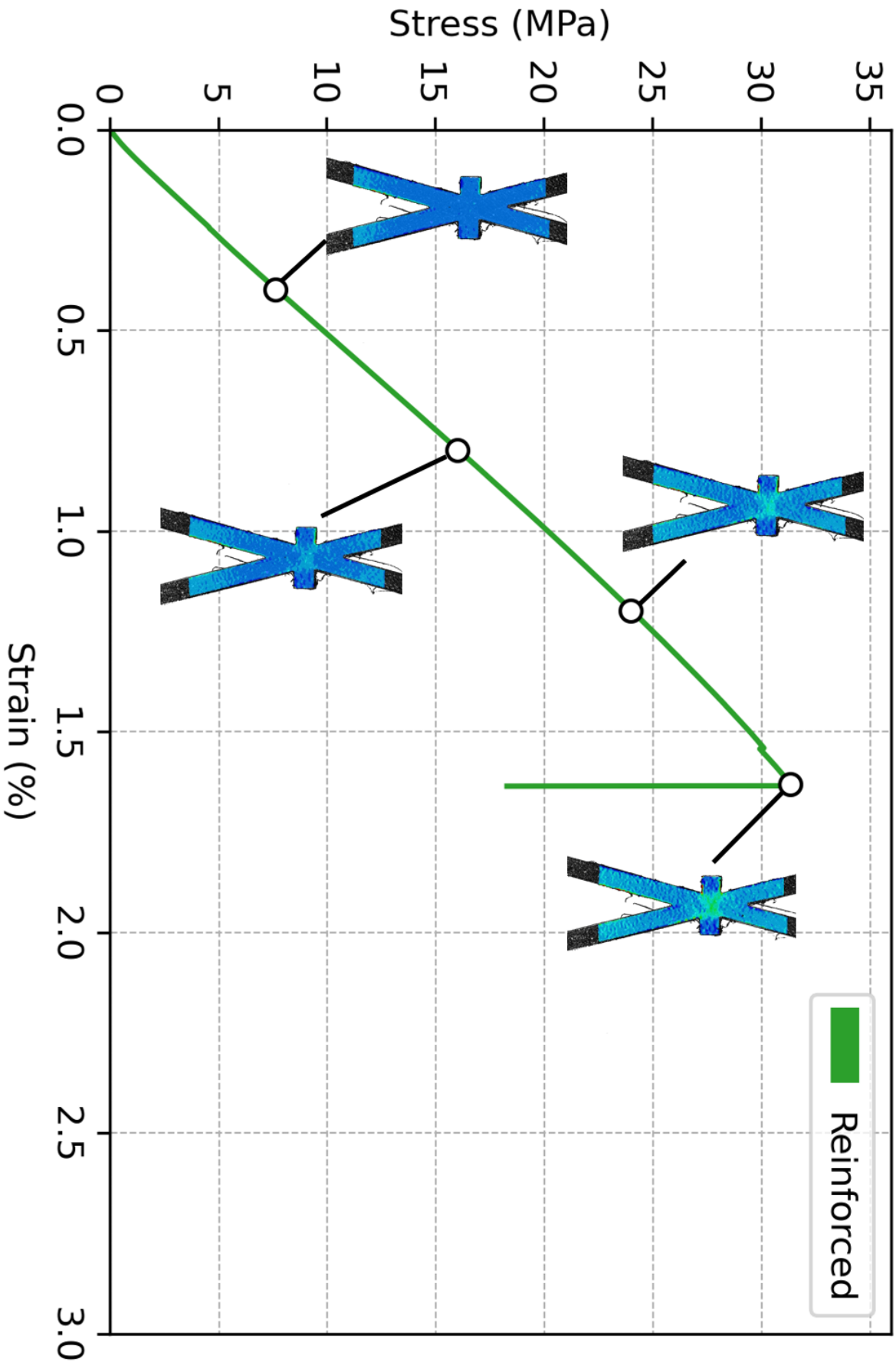

Figure 4.21: Stress-strain curve of reinforced node with 30 degrees rib angle and ϵ_{yy} strain mapping using DIC

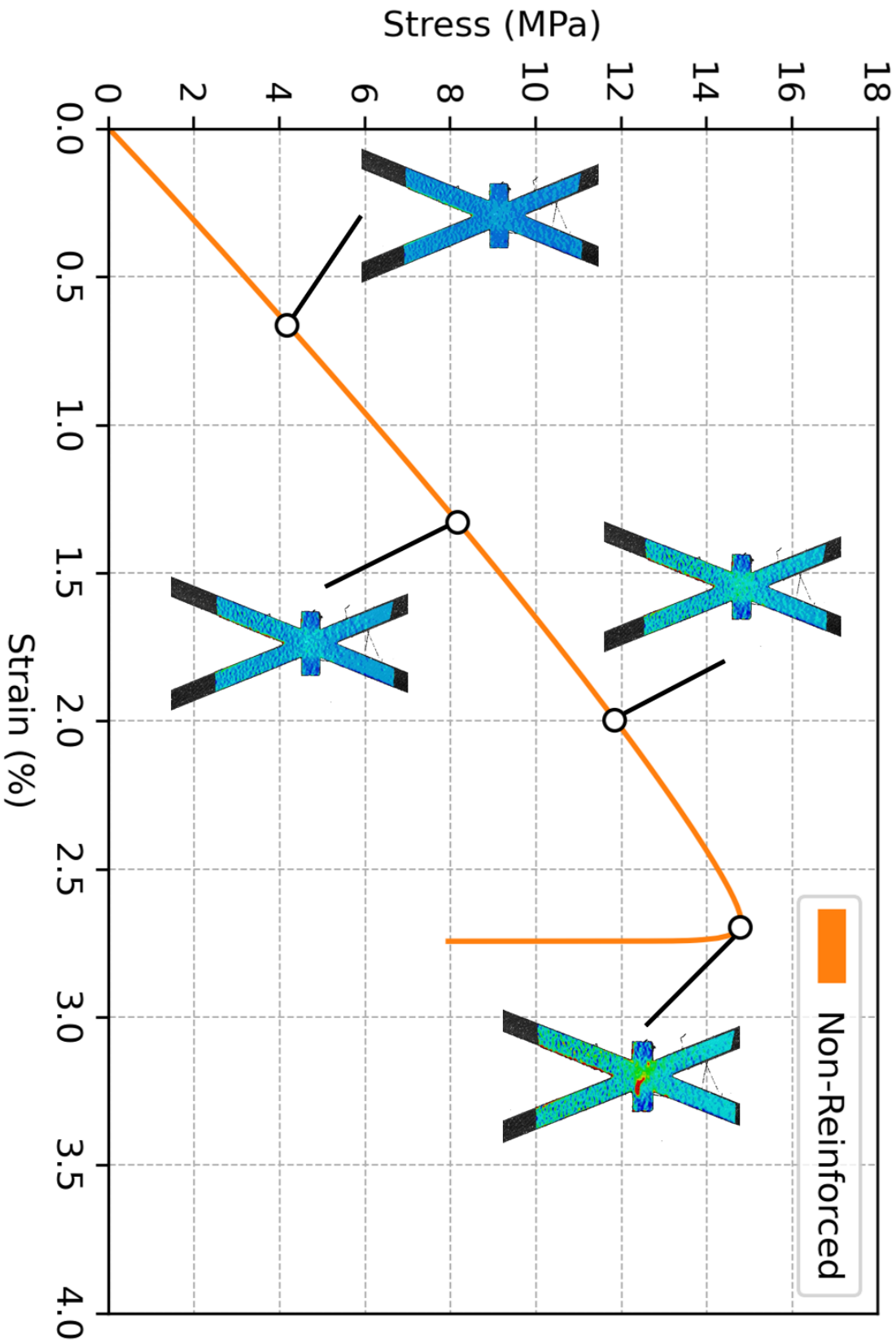

Figure 4.22: Stress-strain curve of non-reinforced node with 45 degrees rib angle and ϵ_{yy} strain mapping using DIC

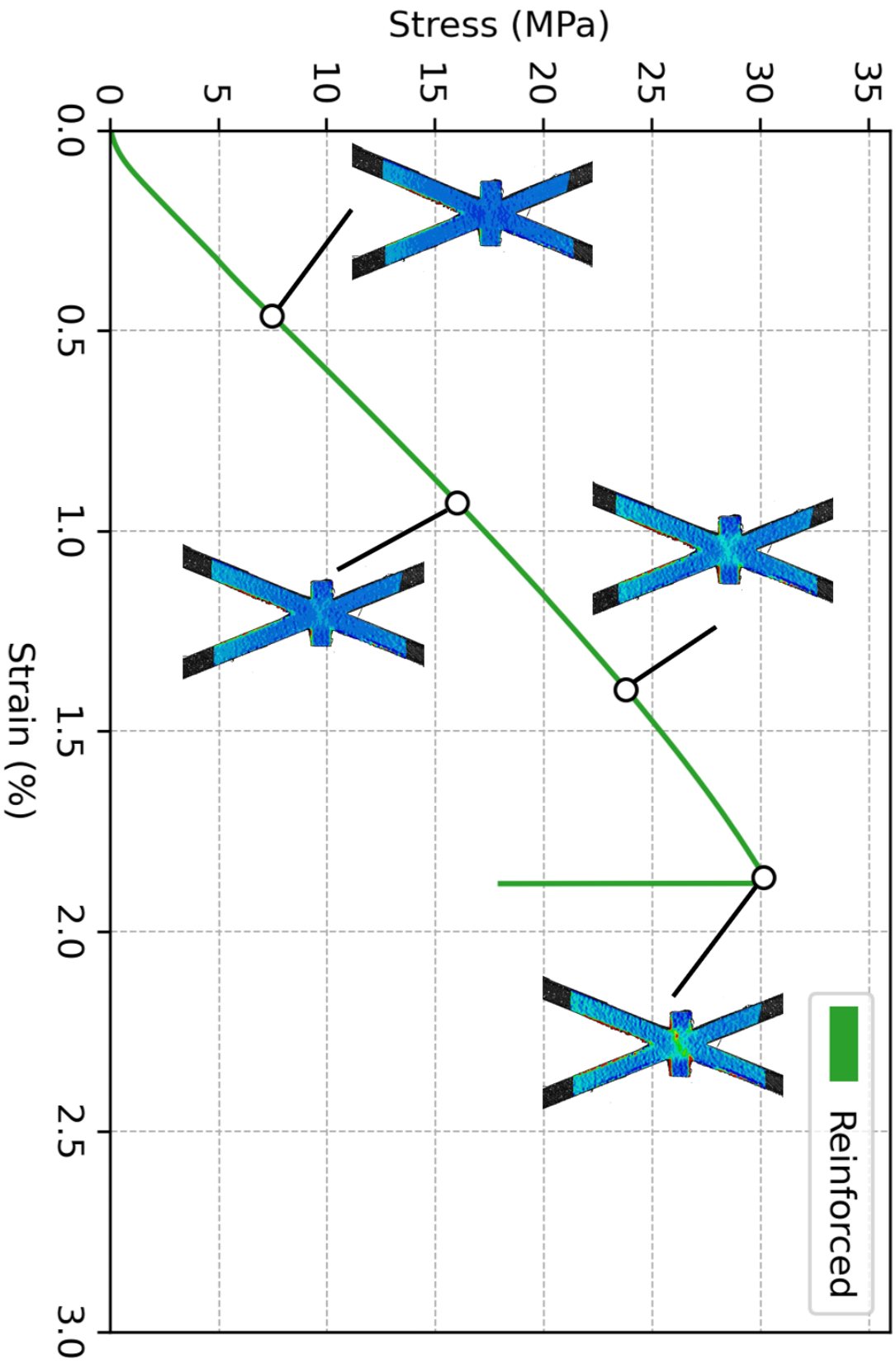

Figure 4.23: Stress-strain curve of non-reinforced node with 45 degrees rib angle and ϵ_{yy} strain mapping using DIC

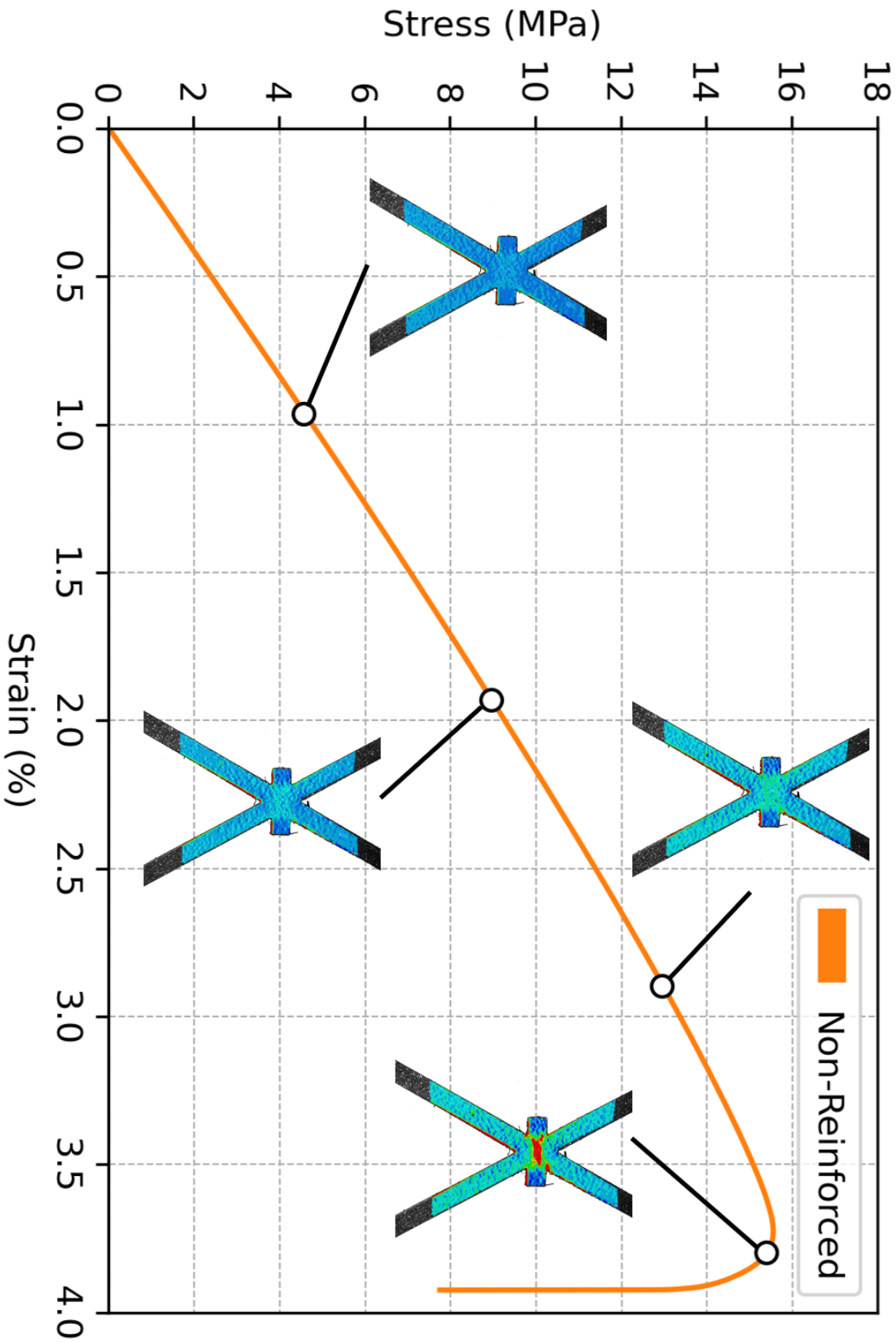

Figure 4.24: Stress-strain curve of non-reinforced node with 60 degrees rib angle and ϵ_{yy} strain mapping using DIC

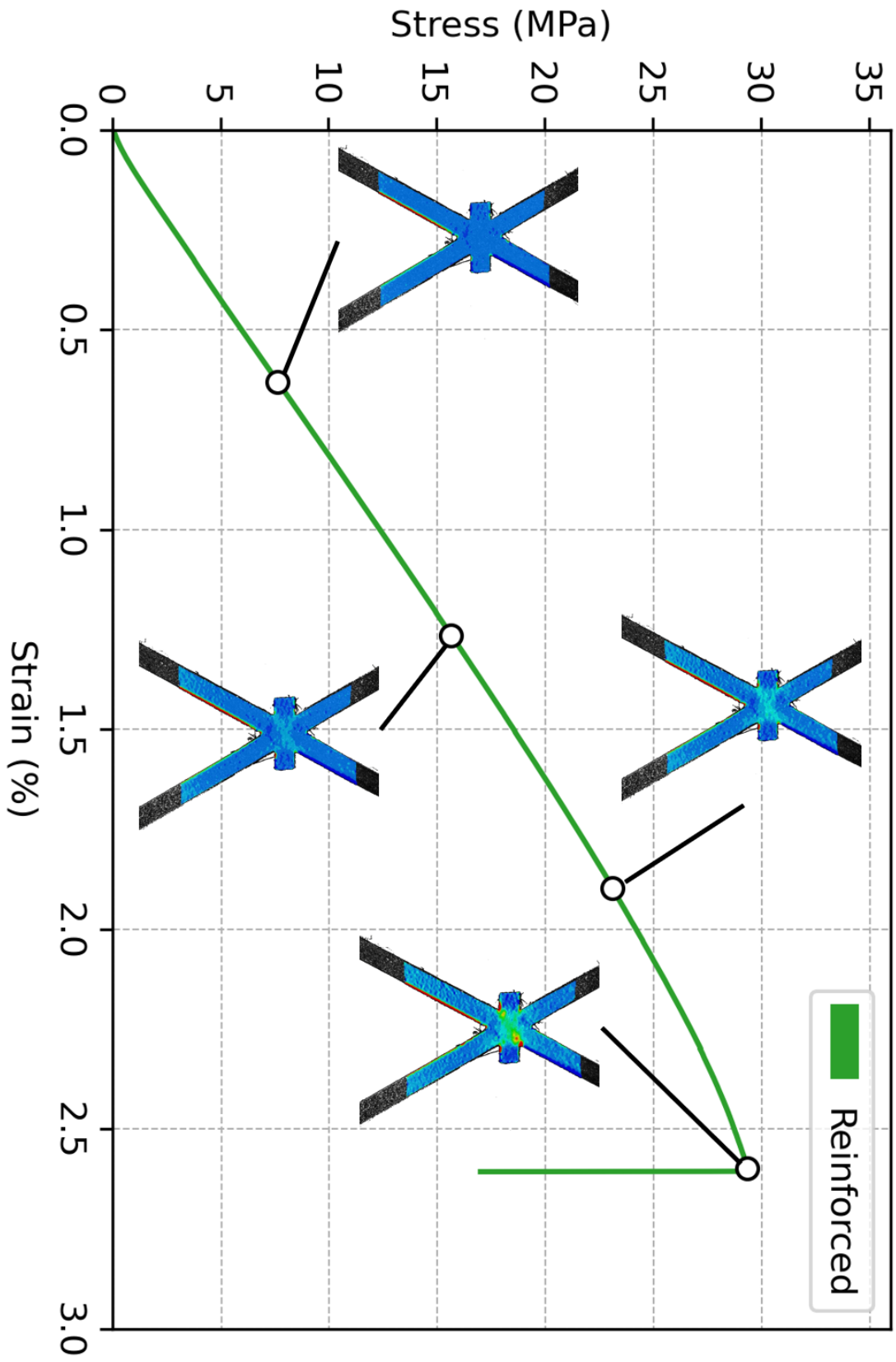

Figure 4.25: Stress-strain curve of reinforced node with 60 degrees rib angle and ϵ_{yy} strain mapping using DIC

4.4 Limitations and Solutions

It is observed that a relatively small addition of fibers (<10%) produces a specimen that is 2x as strong as its pure plastic equivalent. However, the manufacturing process also features disadvantages and limitations that are discussed now. With the Aura software slicer individual fiber lines cannot be drawn. Therefore, the amount of fibers are limited to the width of the specimen. In the specimen produced in this project more than two fiber lines through the ribs are not possible which limits the maximum fiber volume fraction that is achieved. However, it is possible to create a reinforced infill following the isogrid pattern to create a stronger part. Furthermore, compared to its competitors the filament used in this project offers material with the highest fiber volume fraction (60%) [68]. Additionally, considering the size of industrial isogrid structures there is enough space for multiple fibers running through the nodes. Nonetheless, it is something to take into account when shifting to additive manufacturing.

Second of all, the deposition time of the carbon fiber is slow compared to conventional FDM. This is necessary in order to ensure proper impregnation of the fibers and also caused by the stiff characteristics of the carbon fibre filament. Half a gram of the special carbon fibre filament takes half an hour of manufacturing as discussed in section 4.1.2. Considering the large size of the Flying V and the amount of ribs and nodes present this takes a significant amount of time. However, the CFC printer is desktop size and not at all a printer sized for industry. Another solution is to have multiple extruders working simultaneously in order to reduce production time and increase efficiency.

The technique features three axes which produce an object that is limited in dimensions. An aircraft wing is based on an ellipse shape that is impossible to manufacture without the addition of multiple supports. Furthermore, it is necessary to have a large printing bed if it is produced out of one part - something which is desired in order to reduce the number of mechanical connections. A solution to this problem is the robotization of the method which is already the case for FDM. Different projects are executed successfully where an extruder used for conventional 3D printing is installed on the end-manipulator on a robotic arm [69]. With the addition of a robotic arm to the manufacturing process it becomes more flexible, productive and re-configurable. Furthermore, it enables the manufacturing of complex shapes. For the manufacturing of an isogrid structure that follows the shape of the wing a mold with that same shape can be used as printing bed.

Additive manufacturing appears to be an easy manufacturing technique. The print is started after the gcode is uploaded and the next day the product is finished. However, most 3D printers do not feature in-situ quality control. E.g. during one of the prints in this project the specimens detached from the printing bed while the extruder kept printing resulting in a large amount of material waste. Furthermore, a part where one layer completely fails is thrown since it is desired to have an end-product consisting of one piece. In order to overcome this limitation it is necessary to invest in monitoring systems that enable machine learning. One study conducted by Wu *et al.* [70] focused on acoustic emission (AE) to detect errors during the manufacturing process. The authors argue AE is an excellent technique since the signals are processed in real-time and the setup is simple. During the study, the researchers managed to monitor material run-out and clogging of the nozzle. In-situ monitoring systems increase efficiency and reduce maintenance costs when installed correctly.

Another method to additively manufacture composites is with short-fibre reinforced plastics. These materials are covered in section 2 and feature a thermoplastic mixed with chopped up fibers to increase the mechanical strength. Due to time limitations and differences in manufacturing processes this filament is not covered in this study. However, by manufacturing specimens with this material a better comparison can be made how continuous fibers perform related to competitors for isogrids. Furthermore, some studies suggest a combination of short- and continuous fibers is superior for ad-

ditive manufacturing of composites [71]. Additionally, it is interesting to see how the mechanical performance differs if one of the ribs feature discontinuous fibers, since this is the current method of manufacturing grids and nodes with composites.

Research is conducted related to CFC and presence of voids. Vaudémont and Perrin [64] argue that porosity is an issue for CFC due to hot formability and multi-material adhesion issues. Therefore, it is recommended to use the same thermoplastic filament for both nozzles in the extruder. However, voids remain an issue as discussed in the study aforementioned. The researchers managed to produce a new filament in combination with a different epoxy resin where a significant reduction in cracks and voids was observed in the filament compared to the CCF. A different study investigated the linear-elastic behavior of a specimen manufactured with continuous fibers. The researchers discovered a deviation between the simulated and actual mechanical behavior of the samples [72]. The authors concluded that the difference is caused by voids hindering the transmission of force.

4.4.1 Expectations

The specimens in this project are exposed to tensile tests. However, wings in aircraft endure more forces during flight such as compression and bending. Although those tests are not executed, a prediction can be made on their behavior.

The largest problem with compression of composites is buckling - where the fibers start to bend perpendicular to the force due to excess stress [73]. Zeng *et al.* [74] discovered that honeycomb structures manufactured with continuous fibers outperform other competitors in terms of compression strength and energy absorption. The researchers discovered that although the layer-by-layer manufacturing caused plastic cracking on the outside, the bonding performance ensured a significant increase in strength. It was concluded that continuous fibers provide the potential to produce structures with high energy absorption.

As discussed in the introduction a typical wing structure consists of ribs and a skin. In this project only the ribs are tested. However, the skin adds a significant amount of strength and stiffness to the overall structure. It is possible to create the rib-skin configuration in one part through the additive manufacturing technology. One proposal is to produce the skin with a regular reinforced isogrid infill (an infill based on carbon fibre filament) while using continuous carbon fibre + reinforced infill in the ribs for maximum mechanical performance.

4.5 End Discussion

The initial idea of this project is to verify if the concept of continuous fibers through all ribs is a feasible technology for the manufacturing of isogrid structures. The technique used here has one large advantage over alternative methods - the absence of fiber pile up in the middle of the node.

The technology works as proven in the results. It follows the fiber paths that are predicted by the slicer software and there is indeed no fiber pile up in the node. Customization is also possible through different software, where each individual fiber path can be drawn manually - opening up endless possibilities. Furthermore, the advantage mentioned above where multiple fiber lines can cross each other enables the fiber volume fraction to be higher locally compared to traditional manufacturing methods. Additionally, the strength of each rib is equal assuming perfect printing quality due to the presence of the continuous fibers.

A term often mentioned within additive manufacturing is topology optimization. It is described by Rosinha *et al.* [75] as: "(...) a mathematical method which spatially optimizes the distribution

of material within a defined domain, by fulfilling given constraints previously established and minimizing a predefined cost function." The method provides an optimum design in terms of mechanical performance and material costs. Additive manufacturing enables the production of complex shapes that cannot be achieved through current technologies. Perhaps the lattice structure is not the strongest structure in terms of mechanical behavior and it needs to be redesigned through topology optimization - e.g. a design where the ribs follow the complexity and shape of the wing of the Flying V.

4.6 Summary

In this project 31 specimens were subjected to tensile testing and analysis in order to determine the manufacturability of isogrids by means of additive manufacturing. The printing quality appeared to be good with no defects visible with the naked eye. CT scanning revealed stringing on some spots, but no layer defects were observed. Furthermore, more than 95% of the fibers were laid down in the desired direction. The fiber volume content in the whole specimen was calculated at around 7% for all specimens. This V_f provided a specimen two times as strong as its pure plastic equivalent. Furthermore, through DIC and extensometer analysis it was concluded that a reinforced specimen is stiffer. The results seem promising, but there are some limitation to the manufacturing process. First of all, the reinforcement in the direction of the rib is limited to the width of it. Furthermore, it is a slow process that has no in-situ monitoring and creates voids in the end product. However, with the introduction of Industry 4.0 and machine learning it is possible to invest in closed-loop monitoring systems in order to increase efficiency and reduce maintenance costs. The time constraint can be solved by implementing (multiple) robotic arms each featuring a special composite extruder. Lastly, it is difficult to put this technique in perspective as it is required to manufacture different configurations e.g. short-fibre or discontinuous fibers. However, the technique offers one large advantage over all its competitors - the possibility to have overlapping fibers without the excessive material build-up. This is caused by the consolidation of the fiber that ensures thinner fibers locally to keep the thickness of the layer constant. Compared to traditional methods, it is possible to have higher fiber volume fraction at the nodal points - the weakest points of an isogrid structure.

5 | Conclusion

Climate change is a topic that is raising awareness in all sectors including aviation. In order to reduce the impact of the aviation industry on climate change a new design is required made of composite material. A typical way to increase structural strength is through the manufacturing of grid structures. This thesis aimed to determine the feasibility of additive manufacturing for the production of grid structures. The thesis focused on the following areas:

- The advantages and disadvantages of current manufacturing techniques of grid structures;
- Methods to create composite structures through additive manufacturing;
- The impact of additive manufacturing on structural behavior of grid structures;
- The challenges and limitations of the proposed method.

The technique introduced in this thesis offers the possibility of having continuous fibers through all ribs in a lattice structure - eliminating one of the largest disadvantages of traditional manufacturing methods of isogrids. The new manufacturing method is based on impregnating the carbon fibre filament with PETG on the printing bed, following the fibre paths determined by the slicer software. Six different configurations were manufactured and exposed to testing. The tensile tests that were executed showed a significant increase in strength and stiffness for the reinforced specimens with a fiber volume content lower than 10%. CT scans showed expected manufacturing quality, with only limited amounts of stringing and the fiber paths >95% in the direction of the ribs. Through this testing it was discovered that this AM technique offers great potential for the manufacturing of ribs.

However, CFC has disadvantages. First of all, it is rather slow due to the impregnation time and stiff characteristics of the filament. Second of all, there is no in-situ monitoring at the moment which can cause material waste in case of malfunctions. Furthermore, complex shapes are difficult to achieve with this printing setup without having a large amount of support structures. However, there is solutions to all these limitations and these are of secondary importance.

The largest advantage of the method for manufacturing in this thesis is that of consolidation of the fibers. This ensures that fibers overlap each other without fiber pile up. Not only does this make it possible to manufacturing grid structures, but it also ensures that the fiber fraction can reach higher numbers compared to traditional manufacturing methods.

Future research should focus on alternatives for additive manufacturing of composites e.g. short fibres. These should be manufactured using the same printer and parameters as the other specimens to get an accurate result of the effect of the material. Other ideas are to use a software called Nano-CAD where fibre paths can be drawn manually. An accurate comparison can then be made between a specimen with continuous and discontinuous fibres in the node. However, this requires highly-skilled professionals as it is a complex software. In the future, a researcher should focus on determining the optimal parameters in terms of surface quality and mechanical performance. In the Aura slicer software a custom profile can be made where all printing parameters can be altered. A special software can be used to simulate how the part is manufactured with a focus on internal stresses and warping. Lastly, is important to be able to simulate the behavior of continuous fibres so large structures can be checked for their behavior if manufactured with this technique. However, this requires professionals experienced in simulation of structures and material as this is highly complex.

Bibliography

[1] M. Kılıç, A. Uyar and A. S. Karaman, 'What impacts sustainability reporting in the global aviation industry? an institutional perspective,' *Transport Policy*, vol. 79, pp. 54–65, 2019.

[2] A. W. Schäfer and I. A. Waitz, 'Air transportation and the environment,' *Transport Policy*, vol. 34, pp. 1–4, 2014.

[3] D. S. Lee, D. W. Fahey, P. M. Forster, P. J. Newton, R. C. Wit, L. L. Lim, B. Owen and R. Sausen, 'Aviation and global climate change in the 21st century,' *Atmospheric Environment*, vol. 43, no. 22-23, pp. 3520–3537, 2009.

[4] A. Bolsunovsky, N. Buzoverya, B. Gurevich, V. Denisov, A. Dunaevsky, L. Shkadov, O. Sonin, A. Udzhuhu and J. Zhurihin, 'Flying wing—problems and decisions,' *Aircraft design*, vol. 4, no. 4, pp. 193–219, 2001.

[5] J. Benad, 'The flying v-a new aircraft configuration for commercial passenger transport,' 2015.

[6] B. Rubio Pascual and R. Vos, 'The effect of engine location on the aerodynamic efficiency of a flying-v aircraft,' in *AIAA Scitech 2020 Forum*, 2020, p. 1954.

[7] R. van der Pluijm, 'Cockpit design and integration into the flying v,' 2021.

[8] F. Faggiano, R. Vos, M. Baan and R. Van Dijk, 'Aerodynamic design of a flying v aircraft,' in *17th AIAA Aviation Technology, Integration, and Operations Conference*, 2017, p. 3589.

[9] H. Wu, C. Lai, F. Sun, M. Li, B. Ji, W. Wei, D. Liu, X. Zhang and H. Fan, 'Carbon fiber reinforced hierarchical orthogrid stiffened cylinder: Fabrication and testing,' *Acta Astronautica*, vol. 145, pp. 268–274, 2018.

[10] A. Forcellese, M. Simoncini, A. Vita and V. Di Pompeo, '3d printing and testing of composite isogrid structures,' *The International Journal of Advanced Manufacturing Technology*, vol. 109, no. 7, pp. 1881–1893, 2020.

[11] G. Francois, J. E. Cooper and P. Weaver, 'Aeroelastic tailoring using rib/spar orientations: Experimental investigation,' in *56th AIAA/ASCE/AHS/ASC Structures, Structural Dynamics, and Materials Conference*, 2015, p. 0439.

[12] S. Van Empelen and R. Vos, 'Effect of engine integration on a 4.6%-scale flying-v subsonic transport,' in *AIAA Scitech 2021 Forum*, 2021, p. 0939.

[13] T. Dotman, 'A structural sizing methodology for the wing-fuselage of the flying-v,' 2021.

[14] T. D. Kim, 'Fabrication and testing of thin composite isogrid stiffened panel,' *Composite structures*, vol. 49, no. 1, pp. 21–25, 2000.

[15] S. M. Huybrechts, S. E. Hahn and T. E. Meink, 'Grid stiffened structures: A survey of fabrication, analysis and design methods,' in *Proceedings of the 12th international conference on composite materials (ICCM/12)*, 1999, pp. 1–10.

[16] V. Vasiliev, V. Barynin and A. Rasin, 'Anisogrid lattice structures–survey of development and application,' *Composite structures*, vol. 54, no. 2-3, pp. 361–370, 2001.

[17] H.-J. Chen and S. W. Tsai, 'Analysis and optimum design of composite grid structures,' *Journal of composite materials*, vol. 30, no. 4, pp. 503–534, 1996.

[18] A. Güemes, E. Del Olmo, M. Dorte and A. Fernandez-Lopez, 'Structural testing and simulation of composite isogrid structures for aerospace applications,' *ECCM15*, 2012.

[19] S. Huybrechts and S. W. Tsai, 'Analysis and behavior of grid structures,' *Composites science and technology*, vol. 56, no. 9, pp. 1001–1015, 1996.

[20] A. Brasington, C. Sacco, J. Halbritter, R. Wehbe and R. Harik, 'Automated fiber placement: A review of history, current technologies, and future paths forward,' *Composites Part C: Open Access*, vol. 6, p. 100 182, 2021.

[21] G. Marsh, 'Automating aerospace composites production with fibre placement,' *REINFORCED plastics*, vol. 55, no. 3, pp. 32–37, 2011.

[22] C. Zhao, M. J. Donough, B. G. Prusty and J. Xiao, 'Influences of ply waviness and discontinuity on automated fibre placement manufactured grid stiffeners,' *Composite Structures*, vol. 256, p. 113 106, 2021.

[23] N. Bakhshi and M. Hojjati, 'Effect of compaction roller on layup quality and defects formation in automated fiber placement,' *Journal of Reinforced Plastics and Composites*, vol. 39, no. 1-2, pp. 3–20, 2020.

[24] H.-J. L. Dirk, C. Ward and K. D. Potter, 'The engineering aspects of automated prepreg layup: History, present and future,' *Composites Part B: Engineering*, vol. 43, no. 3, pp. 997–1009, 2012.

[25] J. Frketic, T. Dickens and S. Ramakrishnan, 'Automated manufacturing and processing of fiber-reinforced polymer (frp) composites: An additive review of contemporary and modern techniques for advanced materials manufacturing,' *Additive Manufacturing*, vol. 14, pp. 69–86, 2017.

[26] M. Di Francesco, L. Veldenz, G. Dell'Anno and K. Potter, 'Heater power control for multi-material, variable speed automated fibre placement,' *Composites Part A: Applied Science and Manufacturing*, vol. 101, pp. 408–421, 2017.

[27] N. Bakhshi and M. Hojjati, 'Time-dependent wrinkle formation during tow steering in automated fiber placement,' *Composites Part B: Engineering*, vol. 165, pp. 586–593, 2019.

[28] M. Quanjin, M. Rejab, M. Idris, N. M. Kumar and M. Merzuki, 'Robotic filament winding technique (rfwt) in industrial application: A review of state of the art and future perspectives,' *Int. Res. J. Eng. Technol*, vol. 5, no. 12, pp. 1668–1676, 2018.

[29] A. Azarov, V. Kolesnikov and A. Khaziev, 'Development of equipment for composite 3d printing of structural elements for aerospace applications,' in *IOP Conference Series: Materials Science and Engineering*, IOP Publishing, vol. 934, 2020, p. 012 049.

[30] F. Abdalla, S. Mutasher, Y. Khalid, S. Sapuan, A. Hamouda, B. Sahari and M. Hamdan, 'Design and fabrication of low cost filament winding machine,' *Materials & design*, vol. 28, no. 1, pp. 234–239, 2007.

[31] T. Centea, L. K. Grunenfelder and S. R. Nutt, 'A review of out-of-autoclave prepregs–material properties, process phenomena, and manufacturing considerations,' *Composites Part A: Applied Science and Manufacturing*, vol. 70, pp. 132–154, 2015.

[32] H. Zhang, T. Huang, Q. Jiang, L. He, A. Bismarck and Q. Hu, 'Recent progress of 3d printed continuous fiber reinforced polymer composites based on fused deposition modeling: A review,' *Journal of Materials Science*, vol. 56, no. 23, pp. 12 999–13 022, 2021.

[33] M. Araya-Calvo, I. López-Gómez, N. Chamberlain-Simon, J. L. León-Salazar, T. Guillén-Girón, J. S. Corrales-Cordero and O. Sánchez-Brenes, 'Evaluation of compressive and flexural properties of continuous fiber fabrication additive manufacturing technology,' *Additive Manufacturing*, vol. 22, pp. 157–164, 2018.

[34] S. F. Kabir, K. Mathur and A.-F. M. Seyam, 'A critical review on 3d printed continuous fiber-reinforced composites: History, mechanism, materials and properties,' *Composite Structures*, vol. 232, p. 111 476, 2020.

[35] W. Chen, Q. Zhang, H. Cao and Y. Yuan, 'Process evaluation, tensile properties, mathematical models, and fracture behavior of 3d printed continuous fiber reinforced thermoplastic composites,' *Journal of Reinforced Plastics and Composites*, vol. 40, no. 21-22, pp. 845–863, 2021.

[36] M. Luo, X. Tian, J. Shang, W. Zhu, D. Li and Y. Qin, 'Impregnation and interlayer bonding behaviours of 3d-printed continuous carbon-fiber-reinforced poly-ether-ether-ketone composites,' *Composites Part A: Applied Science and Manufacturing*, vol. 121, pp. 130–138, 2019.

[37] J. Zhang, Z. Zhou, F. Zhang, Y. Tan, Y. Tu and B. Yang, 'Performance of 3d-printed continuous-carbon-fiber-reinforced plastics with pressure,' *Materials*, vol. 13, no. 2, p. 471, 2020.

[38] T. Liu, X. Tian, Y. Zhang, Y. Cao and D. Li, 'High-pressure interfacial impregnation by microscrew in-situ extrusion for 3d printed continuous carbon fiber reinforced nylon composites,' *Composites Part A: Applied Science and Manufacturing*, vol. 130, p. 105 770, 2020.

[39] Z. Hou, X. Tian, Z. Zheng, J. Zhang, L. Zhe, D. Li, A. V. Malakhov and A. N. Polilov, 'A constitutive model for 3d printed continuous fiber reinforced composite structures with variable fiber content,' *Composites Part B: Engineering*, vol. 189, p. 107 893, 2020.

[40] G. Liu, 'A step-by-step method of rule-of-mixture of fiber-and particle-reinforced composite materials,' *Composite structures*, vol. 40, no. 3-4, pp. 313–322, 1997.

[41] I. Ferreira, M. Machado, F. Alves and A. T. Marques, 'A review on fibre reinforced composite printing via fff,' *Rapid Prototyping Journal*, 2019.

[42] A. Adumitroaie, F. Antonov, A. Khaziev, A. Azarov, M. Golubev and V. V. Vasiliev, 'Novel continuous fiber bi-matrix composite 3-d printing technology,' *Materials*, vol. 12, no. 18, p. 3011, 2019.

[43] S. Kannan, R. Vezhavendhan, S. Kishore and K. V. Kanumuru, 'Investigating the effect of orientation, infill density with triple raster pattern on the tensile properties for 3d printed samples,' *IOP SciNotes*, vol. 1, no. 2, p. 024 405, 2020.

[44] A. Parmiggiani, M. Prato and M. Pizzorni, 'Effect of the fiber orientation on the tensile and flexural behavior of continuous carbon fiber composites made via fused filament fabrication,' *The International Journal of Advanced Manufacturing Technology*, vol. 114, no. 7, pp. 2085–2101, 2021.

[45] C. Quan, B. Han, Z. Hou, Q. Zhang, X. Tian and T. J. Lu, '3d printed continuous fiber reinforced composite auxetic honeycomb structures,' *Composites Part B: Engineering*, vol. 187, p. 107 858, 2020.

[46] A. Azarov, V. Vasiliev, A. Razin, V. Salov and D. Kotlov, 'Composite reinforcing thread, prepreg, tape for 3-d printing and instalation for preparing same,' *Anisoprint Patent No. WO*, vol. 188861, A1, 2017.

[47] A. Uşun and R. Gümrük, 'The mechanical performance of the 3d printed composites produced with continuous carbon fiber reinforced filaments obtained via melt impregnation,' *Additive Manufacturing*, vol. 46, p. 102 112, 2021.

[48] E. García, P. Núñez, M. Caminero, J. Chacón and S. Kamarthi, 'Effects of carbon fibre reinforcement on the geometric properties of petg-based filament using fff additive manufacturing,' *Composites Part B: Engineering*, vol. 235, p. 109 766, 2022, ISSN: 1359-8368.

[49] M. S. Alsoufi and A. Elsayed, 'Warping deformation of desktop 3d printed parts manufactured by open source fused deposition modeling (fdm) system,' *Int. J. Mech. Mechatron. Eng*, vol. 17, no. 11, 2017.

[50] D. Brion, M. Shen and S. Pattinson, 'Automated recognition and correction of warp deformation in extrusion additive manufacturing,' *Additive Manufacturing*, p. 102 838, 2022.

[51] B. Shaqour, M. Abuabiah, S. Abdel-Fattah, A. Juaidi, R. Abdallah, W. Abuzaina, M. Qarout, B. Verleije and P. Cos, 'Gaining a better understanding of the extrusion process in fused filament fabrication 3d printing: A review,' *The International Journal of Advanced Manufacturing Technology*, vol. 114, no. 5, pp. 1279–1291, 2021.

[52] A. Qattawi, M. A. Ablat *et al.*, 'Design consideration for additive manufacturing: Fused deposition modelling,' *Open Journal of Applied Sciences*, vol. 7, no. 6, pp. 291–318, 2017.

[53] H. Baş, S. Elevli and F. Yapıcı, 'Fault tree analysis for fused filament fabrication type three-dimensional printers,' *Journal of Failure Analysis and Prevention*, vol. 19, no. 5, pp. 1389–1400, 2019.

[54] S. K. Everton, M. Hirsch, P. Stravroulakis, R. K. Leach and A. T. Clare, 'Review of in-situ process monitoring and in-situ metrology for metal additive manufacturing,' *Materials & Design*, vol. 95, pp. 431–445, 2016.

[55] I. Arbnor and B. Bjerke, *Methodology for creating business knowledge*. Sage, 2008.

[56] S. Garbarino and J. Holland, 'Quantitative and qualitative methods in impact evaluation and measuring results,' 2009.

[57] M. Bruyneel, J.-P. Delsemme, A.-C. Goupil, P. Jetteur, C. Lequesne, T. Naito and Y. Urushiyama, 'Damage modeling of laminated composites: Validation of the intra-laminar damage law of samcef at the coupon level for ud plies,' in *proceedings of the European Conference on Composite Material, ECCM16*, 2014.

[58] K. Durgashyam, M. I. Reddy, A. Balakrishna and K. Satyanarayana, 'Experimental investigation on mechanical properties of petg material processed by fused deposition modeling method,' *Materials Today: Proceedings*, vol. 18, pp. 2052–2059, 2019.

[59] F. Liu, E. Ferraris and J. Ivens, 'Mechanical investigation and microstructure performance of a two-matrix continuous carbon fibre composite fabricated by 3d printing,' *Journal of Manufacturing Processes*, vol. 79, pp. 383–393, 2022.

[60] Y. Nikishkov, L. Airoldi and A. Makeev, 'Measurement of voids in composites by x-ray computed tomography,' *Composites Science and Technology*, vol. 89, pp. 89–97, 2013.

[61] S. Garcea, Y. Wang and P. Withers, 'X-ray computed tomography of polymer composites,' *Composites Science and Technology*, vol. 156, pp. 305–319, 2018.

[62] M. El Messiry, 'Theoretical analysis of natural fiber volume fraction of reinforced composites,' *Alexandria Engineering Journal*, vol. 52, no. 3, pp. 301–306, 2013.

[63] H. Lim and S. W. Hoag, 'Plasticizer effects on physical–mechanical properties of solvent cast soluplus® films,' *Aaps Pharmscitech*, vol. 14, no. 3, pp. 903–910, 2013.

[64] R. Vaudémont and H. Perrin, 'Assessment of reactive thermoplastic composite pultrusion for continuous-fibre reinforced 3d printing,' 2020.

[65] Anisoprint LLC, 'Safety data sheet ccf,' 2018. [Online]. Available: `https://ballistic-bit.com/Files/SDS-CCF-Anisoprint.pdf`.

[66] F. Taheri-Behrooz, M. M. Shokrieh and H. Sokhanvar, 'A new model for the determination of optimum fiber volume fraction under multi-axial loading in polymeric composites,' *Iranian Polymer Journal*, vol. 28, no. 1, pp. 31–38, 2019.

[67] H.-w. He and F. Gao, 'Effect of fiber volume fraction on the flexural properties of unidirectional carbon fiber/epoxy composites,' *International Journal of Polymer Analysis and Characterization*, vol. 20, no. 2, pp. 180–189, 2015.

[68] D. Pezold, T. Rosnitschek, A. Kleuderlein, F. Döpper and B. Alber-Laukant, 'Evaluation of technologies for the fabrication of continuous fiber reinforced thermoplastic parts by fused layer modeling,' in *Technologies for economic and functional lightweight design*, Springer, 2021, pp. 125–141.

[69] P. Urhal, A. Weightman, C. Diver and P. Bartolo, 'Robot assisted additive manufacturing: A review,' *Robotics and Computer-Integrated Manufacturing*, vol. 59, pp. 335–345, 2019.

[70] H. Wu, Y. Wang and Z. Yu, 'In situ monitoring of fdm machine condition via acoustic emission,' *The International Journal of Advanced Manufacturing Technology*, vol. 84, no. 5, pp. 1483–1495, 2016.

[71] Y. Peng, Y. Wu, K. Wang, G. Gao and S. Ahzi, 'Synergistic reinforcement of polyamide-based composites by combination of short and continuous carbon fibers via fused filament fabrication,' *Composite Structures*, vol. 207, pp. 232–239, 2019.

[72] A. Matschinski, D. Bublitz, T. Ihring, C. Y. Chen, S. Grandl, K. Schneider, G. Pearce and K. Drechsler, 'Optimization of continuous fiber path planning for an additively manufactured open-hole specimen,' in *Materials Science Forum*, Trans Tech Publ, vol. 1060, 2022, pp. 127–132.

[73] T. Odijk, 'Microfibrillar buckling within fibers under compression,' *The Journal of chemical physics*, vol. 108, no. 16, pp. 6923–6928, 1998.

[74] C. Zeng, L. Liu, W. Bian, J. Leng and Y. Liu, 'Compression behavior and energy absorption of 3d printed continuous fiber reinforced composite honeycomb structures with shape memory effects,' *Additive Manufacturing*, vol. 38, p. 101 842, 2021.

[75] I. P. Rosinha, K. V. Gernaey, J. M. Woodley and U. Krühne, 'Topology optimization for biocatalytic microreactor configurations,' in *Computer Aided Chemical Engineering*, vol. 37, Elsevier, 2015, pp. 1463–1468.

A | Additional Material

A.1 Prototype on Prusa Printer

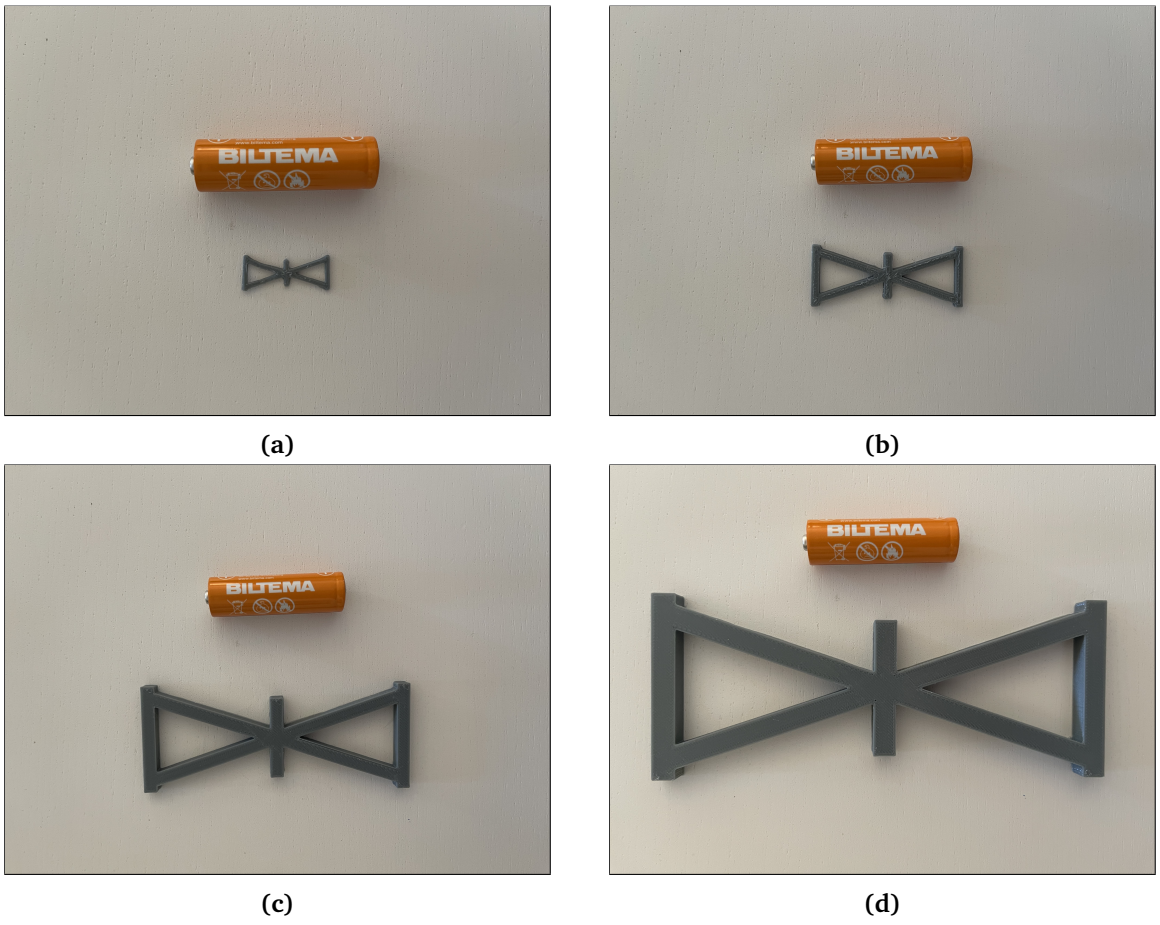

(a) (b) (c) (d)

Figure A.1: (a) First, (b) second, (c) third, and (d) fourth prototype print

A.2 Load-Displacement Curves

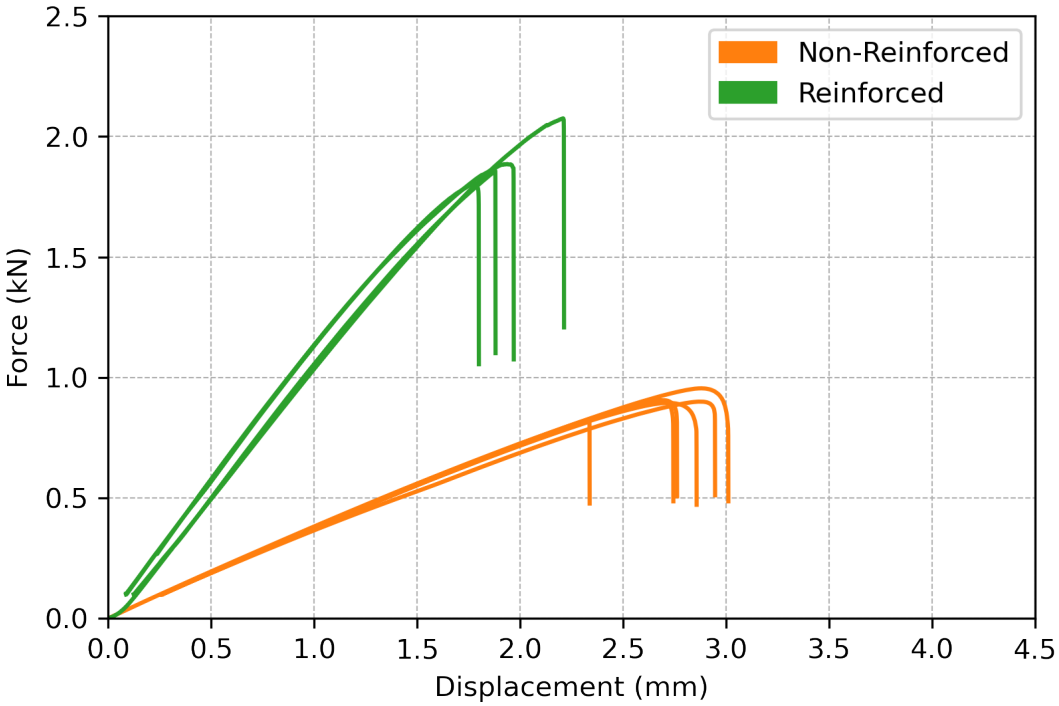

Figure A.2: Load-displacement curve of nodes with 45 degrees rib angle

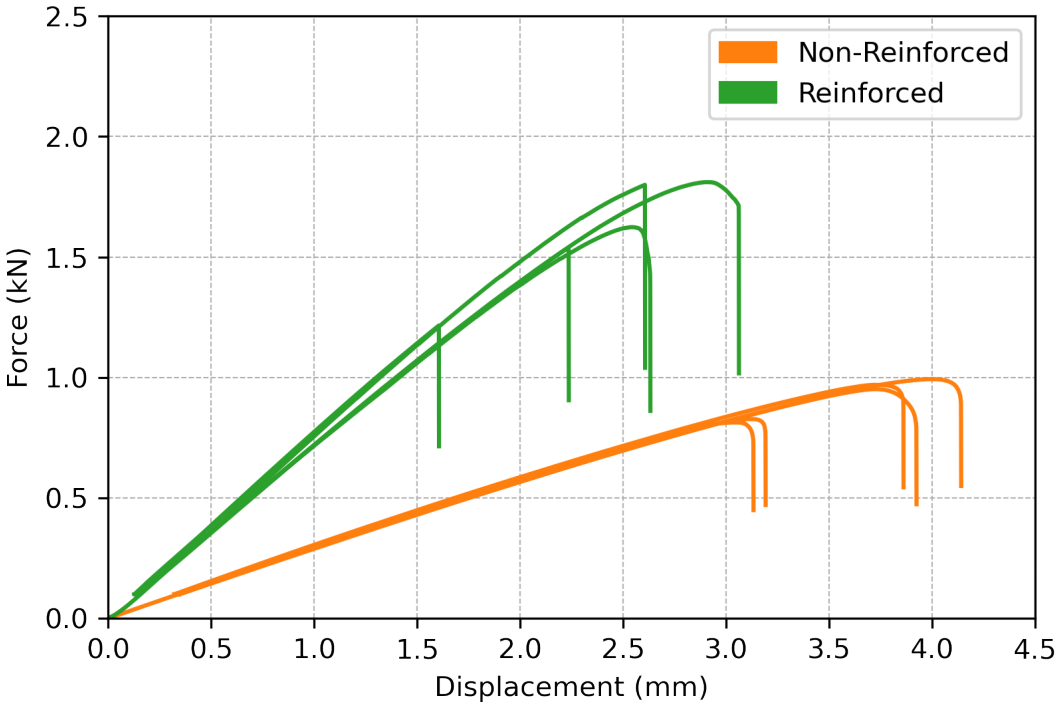

Figure A.3: Load-displacement curve of nodes with 60 degrees rib angle

A.3 Tensile Tests - Results

Table A.1: Results of tensile test

Specimen	Maximum stress (MPa)	Strain at σ_{max} (%)
NR30-1	14.7872	2.9748
NR30-2	15.4234	2.833
NR30-3	15.9467	2.3064
NR30-4	14.5499	2.8542
NR30-5	14.0646	3.0474
NR30-6	15.267	2.4298
R30-1	30.2593	2.3125
R30-2	30.7942	2.0628
R30-3	28.592	2.5204
R30-4	34.9536	2.4227
R30-5	31.3464	1.6305
NR45-1	15.1584	3.0257
NR45-2	12.9649	1.6471
NR45-3	14.2819	2.868
NR45-4	14.3714	2.886
NR45-5	14.1938	2.9743
NR45-6	14.7803	2.696
R45-1	29.9353	3.6973
R45-2	28.6554	2.625
R45-3	32.9415	3.3422
R45-4	30.178	1.8639
NR60-1	12.915	2.466
NR60-2	15.7641	3.4244
NR60-3	15.3889	3.1008
NR60-4	13.1346	2.8855
NR60-5	15.4073	3.7959
R60-1	25.7766	2.2696
R60-2	24.4202	1.543
R60-3	19.2925	1.0496
R60-4	28.7437	3.0634
R60-5	29.3585	2.5976

A.4 Simulation Results

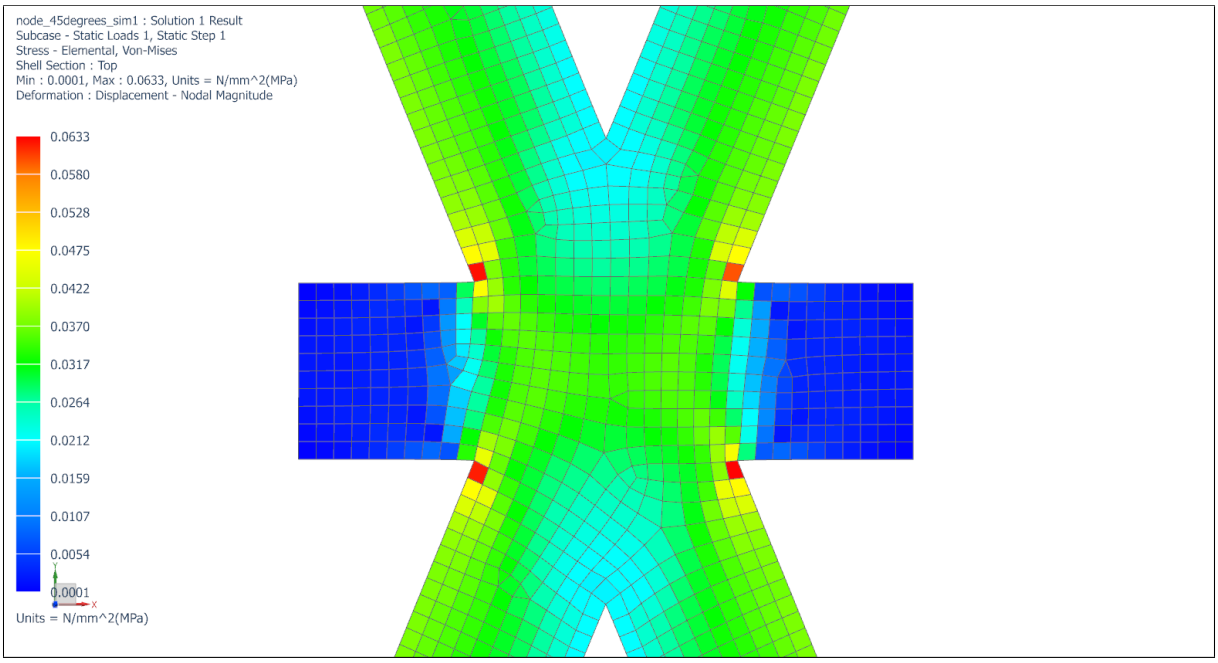

Figure A.4: Von Mises result of simulation of tensile test with 45 degrees rib configuration

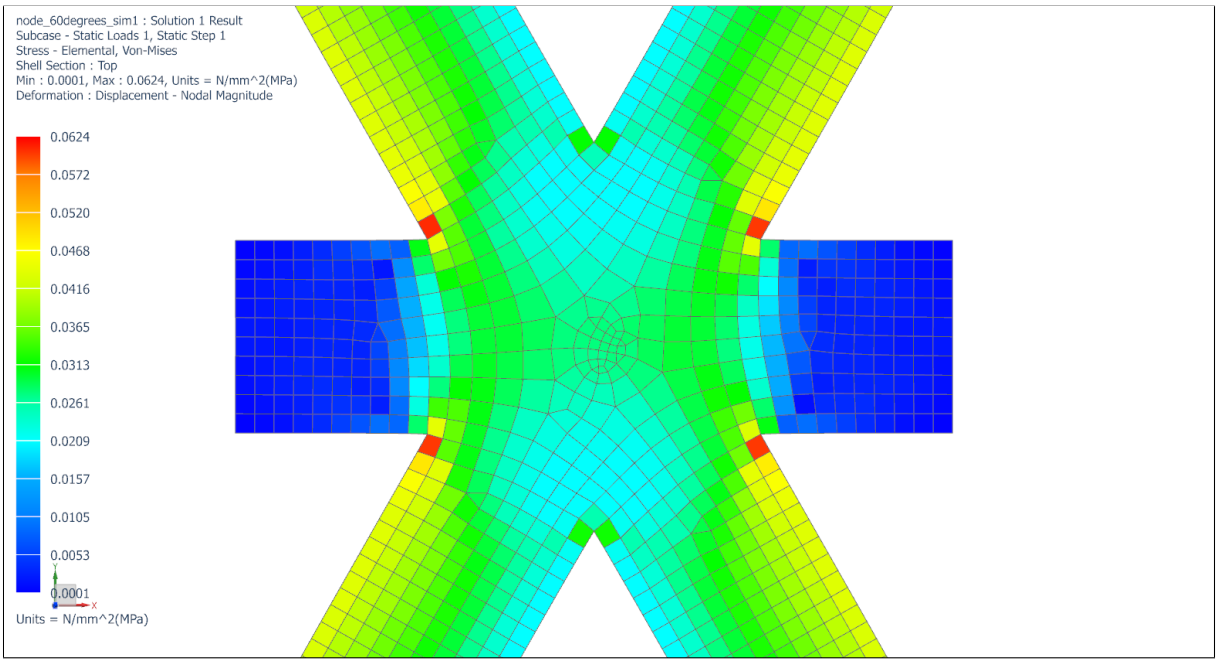

Figure A.5: Von Mises result of simulation of tensile test with 60 degrees rib configuration